

# Variational Asymptotic Homogenization of Finitely Deformed Viscoelastic-Viscoplastic Composites

Liang Zhang\*

*AnalySwift LLC, West Jordan, UT 84081, USA*

Juan M. Fernandez<sup>†</sup> and Andrew Bergan<sup>‡</sup>

*NASA Langley Research Center, Hampton, VA 23681-2199, USA*

Wenbin Yu<sup>§</sup>

*Purdue University, West Lafayette, IN 47907-2045, USA*

The objective of this paper is to develop a constitutive model for finitely deformed viscoelastic-viscoplastic materials and a micromechanics approach to homogenizing composites consisting of such materials. The development of the constitutive model involves establishing a thermodynamic framework based on finite strain theory, developing a viscoelasticity and a viscoplasticity model based on the thermodynamic framework, developing a radial return algorithm based on a classic framework, and deriving a closed-form incremental constitutive relation in the spatial configuration. The development of the micromechanics approach involves pulling-back the above constitutive relation to the material configuration, formulating a variational statement with the resulting constitutive relation, discretizing variational statement in a finite-dimensional space, and solving the discretized variational statement using an Euler–Newton predictor–corrector method. The constitutive model is calibrated via monotonic uniaxial compression tests on a polymer, and the calibrated model is validated by comparing its predictions with the cyclic test data. It is shown capable of characterizing viscoelasticity, viscoplasticity, and complex loading paths. The micromechanics approach’s capabilities are demonstrated through homogenizing a unidirectional fiber-reinforced composite, subjected to uniaxial, biaxial, and shear loading, at different strain rates. It is demonstrated to be capable of handling rate dependence and complex loading paths. The present framework can be further improved by implementing more sophisticated viscoelasticity and viscoplasticity models in future work.

## I. Introduction

Deployable composite booms are designed to be self-deployed in space after (1) flattened and coiled for stowage and (2) stowed for a long time before launch. Thin-ply high strain composites (TP-HSCs) are widely used in booms thanks to their high strength-to-weight ratios, low manufacturing costs, and ability to sustain large curvatures without failure. Despite these advantages, TP-HSCs in composite booms may be degraded by different mechanisms during boom coiling and stowage so that the composite booms partially recover their cross-sections when deployed. Specifically:

1. When a TP-HSC is bent during boom coiling, its resin matrix may undergo finite, viscoplastic deformation.
2. When a TP-HSC has been stowed for a long time, its resin matrix may undergo considerable stress relaxation.

---

\*Senior Research Scientist.

<sup>†</sup>Research Aerospace Engineer, Structural Dynamics Branch.

<sup>‡</sup>Research Aerospace Engineer, Durability, Damage Tolerance, and Reliability Branch.

<sup>§</sup>Professor, School of Aeronautics and Astronautics, AIAA Associate Fellow.

- Once a TP-HSC is considerably degraded, the composite boom may exhibit reduced bending/torsional stiffness and not be successfully deployed.

It is critical but challenging to predict the extent of viscoplastic deformation/stress relaxation in a TP-HSC. For one thing, there is still a need for a constitutive model for the resin matrix exhibiting material and geometric nonlinearities in practice. For another, the multiscale modeling of a composite boom often spans multiple length scales (e.g. fiber, yarn, ply, laminate, and boom structure in Figure 1). In this paper, focus is placed on (1) the constitutive modeling of finitely deformed viscoelastic-viscoplastic materials and (2) the micromechanical analysis of composites consisting of such materials (e.g., unidirectional fiber-reinforced composites (UDFRCs) and yarns).

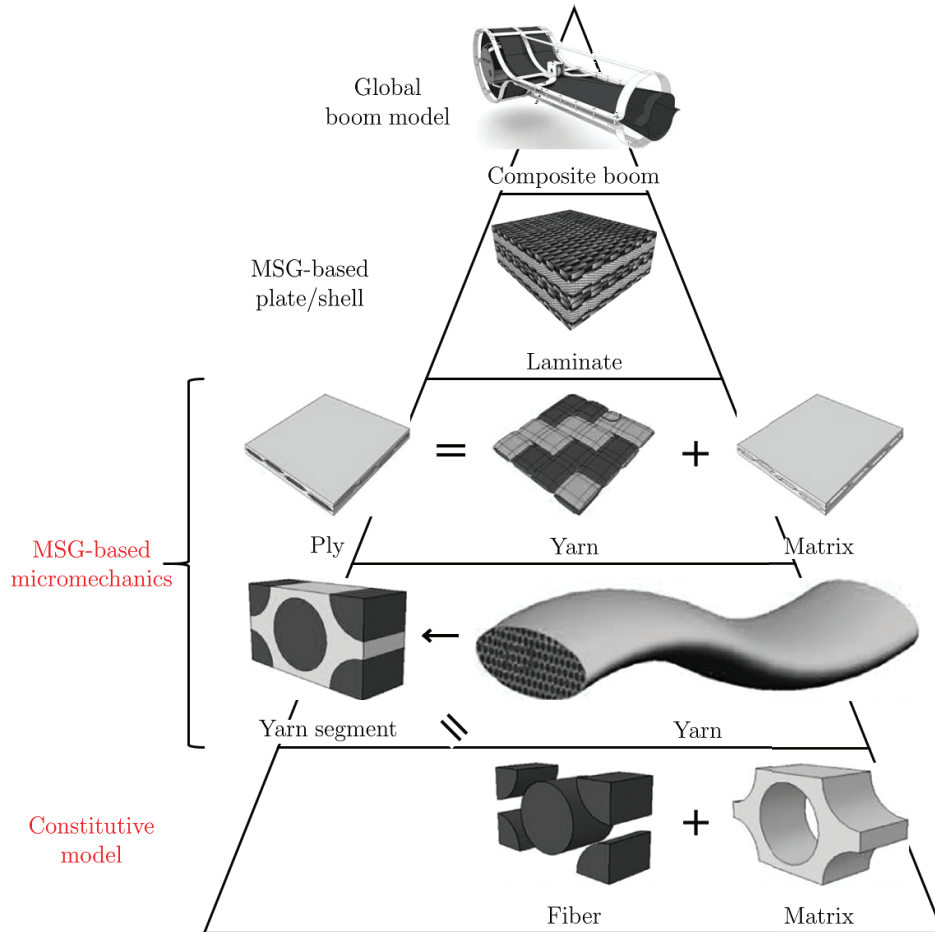


**Figure 1. Bottom-up mechanics of structure genome (MSG)-based multiscale modeling.**

There are only a few recent viscoelastic-viscoplastic constitutive models, and only several of them considered finite strain at the same time. Such a model consists of the stress and the strain measures, a thermodynamic framework, a viscoelasticity model, a viscoplasticity model, a radial return algorithm, and an incremental constitutive relation. Different chosen options on these components result in different constitutive models. It is crucial to properly choose the stress and the strain measures in the finite strain regime. These measures are easy to choose in the infinitesimal strain regime<sup>3,4</sup> or when only considering viscoelasticity.<sup>19</sup> However:

- In finite strain theory, there are multiple combinations of these measures, which result in vastly different thermodynamic frameworks.
- When considering viscoplasticity as well, one must balance between the versatility and complexity of these measures.

On the one hand, simple measures (e.g., the deformation gradients) result in constitutive models (1) easy to develop but (2) incapable of meeting certain requirements (e.g., assumptions and material behavior). On the other hand, complex measures (e.g., nonlinear functions of the deformation gradients) result in constitutive models (1) capable of meeting certain requirements but (2) difficult to develop and to implement in finite element (FE) codes and homogenization frameworks.<sup>1,2</sup> Gudimetla and Doghri<sup>2</sup> stated that the Prony series in viscoelasticity should be defined in the material configuration. To meet this requirement, they chose complex measures but did not obtain a closed-form incremental constitutive relation. In this paper, the simplest possible stress and strain measures are chosen, i.e., they are complex enough to characterize material behavior while simple enough for model development and implementation. Following Ref. [5], the stress and the strain measures are set to be the Kirchhoff stress tensor and the viscoelastic left Cauchy–Green strain tensor, respectively.

In a viscoelasticity model, the strain energy and the branch stress evolution laws must be rigorously formulated. This is because:

- There must be thermodynamic consistency between the viscoelasticity and the viscoplasticity models, and the strain energy ensures this consistency.
- An ad hoc evolution law may result in inaccurate results.

In the infinitesimal strain regime, the evolution laws can be derived by analyzing the branch stresses, and the total stresses can then be expressed as a hereditary integral. In the finite strain regime, several authors<sup>1,2</sup> constructed (not proved) evolution laws, strain energies, and/or stress tensors based on the hereditary integral, introducing thermodynamic inconsistency and/or arbitrariness to their constitutive models. In this paper, the strain energy and the evolution laws are ensured to be rigorous by constructing a 3D viscoelasticity model based on a well established 1D model. When developing viscoplasticity models, some authors<sup>3,4</sup> chose yield functions and flow rules for metals rather than polymers, and others<sup>1,2</sup> chose complex yield functions and/or flow rules, which enhance the difficulties in model calibration. In this paper, the simplest possible yield function and flow rule for polymers are chosen and calibrated via tests.

An integration scheme involves computing, updating, and storing all state variables, in each load step. Radial return is among the most popular integrations schemes for viscoplasticity models. This is because radial return balances accuracy and efficiency well. In the infinitesimal strain regime, the radial return algorithm is well established,<sup>3,4</sup> but in the finite strain regime, it is either absent<sup>2</sup> or very complicated.<sup>2</sup> In this paper, the general radial return algorithm in Ref. [5] is modified to accommodate the current objective, and the viscoelasticity and the viscoplasticity models are implemented in the modified algorithm subsequently. An incremental constitutive relation relates the stress increments to the strain increments. It is needed for the assembly of the global stiffness matrix, during the FE implementation of a constitutive model. Due to the complexity of the problem, none of competing constitutive models has a closed-form incremental constitutive relation. When implementing such a constitutive model, one must accomplish the following:

1. Treat the plastic hardening variables as additional degrees of freedom (DOFs).
2. Customize the FE solver to the additional DOFs.
3. In each load step, solve for the displacements and the plastic hardening variables in a staggered manner.

In this paper, a closed-form incremental constitutive relation is derived and used for model calibration and implementation.

In this paper, homogenization is accomplished using the variational asymptotic homogenization method.<sup>6,7</sup> This method involves asymptotically analyzing a variational statement of a composite and solving the resulting simplified functional equation governing the response of the unit cell. Its first-order approximation is actually mathematically equivalent to the formal asymptotic homogenization method and therefore possesses similar advantages. Since this method is inherently variational, it is straightforward to implement this method using finite element method. Recently, Yu<sup>8</sup> generalized this method to the mechanics of structure genome (MSG), a unified approach to the constitutive modeling of composite structures, based on the concept of structure gene (SG). A structure gene (SG) can be defined as the smallest mathematical building block of a structure. Thanks to SG, MSG can handle a UDFRC subjected to longitudinal shear loading (see Figure 12(b)), with a 2D UC. Zhang and Yu<sup>9,10</sup> extended the MSG-based micromechanics approach for

homogenizing elastoplastic and elasto-viscoplastic composites, and Zhang et al.<sup>11</sup> extended it for homogenizing finitely deformed heterogeneous elastomers. In this paper, the MSG-based micromechanics approach is extended as follows:

1. Pull-back the aforementioned incremental constitutive relation, formulated in the spatial configuration, to the material configuration.
2. Formulate a variational statement with the resulting incremental constitutive relation, in the material configuration (see Section VII for detailed differences).
3. Solve the variational problem in each load step so that the micromechanics approach can handle finitely deformed viscoelastic-viscoplastic composites.

In Ref. [11]:

- The constitutive relation is already formulated in the material configuration, making the above Step 1 unnecessary.
- The variational statement is formulated with a strain energy density function, which does not exist in this paper.

These differences further make the solution procedure of variational problem in this paper different from that in Ref. [11].

This paper is organized as follows. First, a thermodynamic framework is established based on finite strain theory. Then, the general radial return algorithm in Ref. [5] is modified to accommodate the current objective. A viscoelasticity and a viscoplasticity model are developed based on the thermodynamic framework. These models are implemented in the general radial return algorithm. The incremental constitutive relation for the material is first derived in the spatial configuration and then pulled-back to the material configuration. A variational statement of an SG is formulated with the incremental constitutive relation. Then, the variational statement is first discretized in a finite-dimensional space and then solved using an Euler–Newton predictor–corrector method. The constitutive model is calibrated via monotonic uniaxial compression tests on a polymer, and the calibrated model is validated by comparing its predictions with the cyclic test data. The micromechanics approach’s capabilities are demonstrated through homogenizing a UDFRC, subjected to uniaxial, biaxial, and shear loading, at different strain rates.

## II. Thermodynamics

Introduce material coordinates  $\mathbf{X} = (X_1, X_2, X_3)$  and spatial coordinates  $\mathbf{x} = (x_1, x_2, x_3)$ , and let the orthonormal basis of these two sets of coordinates coincide.  $\mathbf{x}$  can be related to  $\mathbf{X}$  and time  $t$  by

$$\mathbf{x}(\mathbf{X}, t) = \mathbf{X} + \mathbf{u}(\mathbf{X}, t), \quad (1)$$

where  $\mathbf{u}(\mathbf{X}, t)$  denotes the displacement vector in the material configuration. The deformation gradient tensor,  $\mathbf{F}$ , is defined as

$$\mathbf{F} = \frac{\partial \mathbf{x}}{\partial \mathbf{X}} = \mathbf{I} + \frac{\partial \mathbf{u}}{\partial \mathbf{X}}, \quad (2)$$

where  $\mathbf{I}$  denotes the second-order identity tensor. The left and the right Cauchy–Green strain tensors,  $\mathbf{b}$  and  $\mathbf{C}$ , are defined as

$$\mathbf{b} = \mathbf{F} \cdot \mathbf{F}^T \quad \text{and} \quad \mathbf{C} = \mathbf{F}^T \cdot \mathbf{F}, \quad (3)$$

respectively. The multiplicative decomposition of  $\mathbf{F}$  into its viscoelastic and viscoplastic parts,  $\mathbf{F}^{ve}$  and  $\mathbf{F}^{vp}$ , reads

$$\mathbf{F} = \mathbf{F}^{ve} \cdot \mathbf{F}^{vp}. \quad (4)$$

The viscoelastic left and the viscoplastic right Cauchy–Green strain tensors,  $\mathbf{b}^{ve}$  and  $\mathbf{C}^{vp}$ , are then

$$\mathbf{b}^{ve} = \mathbf{F}^{ve} \cdot (\mathbf{F}^{ve})^T \quad \text{and} \quad \mathbf{C}^{vp} = (\mathbf{F}^{vp})^T \cdot \mathbf{F}^{vp}, \quad (5)$$

respectively. Combing Eqs. (4) and (5) gives

$$\mathbf{b}^{ve} = \left[ \mathbf{F} \cdot (\mathbf{F}^{vp})^{-1} \right] \cdot \left[ (\mathbf{F}^{vp})^{-T} \cdot \mathbf{F}^T \right] = \mathbf{F} \cdot \left[ (\mathbf{F}^{vp})^{-1} \cdot (\mathbf{F}^{vp})^{-T} \right] \cdot \mathbf{F}^T = \mathbf{F} \cdot (\mathbf{C}^{vp})^{-1} \cdot \mathbf{F}^T. \quad (6)$$

By definition, the Lie derivative of  $\mathbf{b}^{ve}$  reads

$$\mathcal{L}_v \mathbf{b}^{ve} = \mathbf{F} \cdot \frac{\partial}{\partial t} \left( \mathbf{F}^{-1} \cdot \mathbf{b}^{ve} \cdot \mathbf{F}^{-T} \right) \cdot \mathbf{F}^T = \mathbf{F} \cdot \left( \dot{\mathbf{C}}^{vp} \right)^{-1} \cdot \mathbf{F}^T, \quad (7)$$

where the overdot denotes the time derivative of a quantity. Taking time derivatives on both sides of Eq. (6) gives

$$\dot{\mathbf{b}}^{ve} = \mathbf{l} \cdot \mathbf{b}^{ve} + \mathbf{b}^{ve} \cdot \mathbf{l}^T + \mathcal{L}_v \mathbf{b}^{ve}, \quad (8)$$

where  $\mathbf{l} = \dot{\mathbf{F}} \cdot \mathbf{F}^{-1}$  is the spatial velocity gradient.

Let  $\Psi$  denote the Helmholtz free energy per unit volume in the material configuration. It can be treated as a function of a suitable set of independent state variables describing the viscoelasticity and viscoplasticity of the material, e.g.,

$$\Psi = \Psi(\mathbf{b}^{ve}, \gamma_1, \dots, \gamma_N, r), \quad (9)$$

where  $\gamma_i$ 's are strain measures describing viscoelasticity, and  $r$  a scalar describing isotropic hardening. Assume that  $\Psi$  can be decomposed into its viscoelastic and plastic hardening parts, i.e.,

$$\Psi(\mathbf{b}^{ve}, \gamma_1, \dots, \gamma_N, r) = \Psi_{ve}(\mathbf{b}^{ve}, \gamma_1, \dots, \gamma_N) + \Psi_{vp}(r). \quad (10)$$

Taking time derivatives on both sides of Eq. (10) gives

$$\begin{aligned} \dot{\Psi} &= \frac{\partial \Psi}{\partial \mathbf{b}^{ve}} : \left( \mathbf{l} \cdot \mathbf{b}^{ve} + \mathbf{b}^{ve} \cdot \mathbf{l}^T + \mathcal{L}_v \mathbf{b}^{ve} \right) + \sum_{i=1}^N \frac{\partial \Psi}{\partial \gamma_i} : \dot{\gamma}_i + \frac{\partial \Psi}{\partial r} \dot{r} \\ &= \left( 2 \frac{\partial \Psi}{\partial \mathbf{b}^{ve}} \cdot \mathbf{b}^{ve} \right) : \left[ \mathbf{d} + \frac{1}{2} \mathcal{L}_v \mathbf{b}^{ve} \cdot (\mathbf{b}^{ve})^{-1} \right] + \sum_{i=1}^N \frac{\partial \Psi}{\partial \gamma_i} : \dot{\gamma}_i + \frac{\partial \Psi}{\partial r} \dot{r}, \end{aligned} \quad (11)$$

where  $\mathbf{d}$  is the symmetric part of  $\mathbf{l}$ , and the second equality holds due to the symmetry of  $\mathbf{b}^{ve}$ . Substituting Eq. (11) into the Clausius–Duhem inequality gives

$$\begin{aligned} \Phi &= \boldsymbol{\tau} : \mathbf{d} - \dot{\Psi} = \left( \boldsymbol{\tau} - 2 \frac{\partial \Psi}{\partial \mathbf{b}^{ve}} \cdot \mathbf{b}^{ve} \right) : \mathbf{d} \\ &\quad + \left( 2 \frac{\partial \Psi}{\partial \mathbf{b}^{ve}} \cdot \mathbf{b}^{ve} \right) : \left[ -\frac{1}{2} \mathcal{L}_v \mathbf{b}^{ve} \cdot (\mathbf{b}^{ve})^{-1} \right] - \sum_{i=1}^N \frac{\partial \Psi}{\partial \gamma_i} : \dot{\gamma}_i - \frac{\partial \Psi}{\partial r} \dot{r} \geq 0, \end{aligned} \quad (12)$$

where  $\Phi$  denotes the dissipation per unit volume, and  $\boldsymbol{\tau}$  the Kirchhoff stress tensor ( $\boldsymbol{\tau} = J\boldsymbol{\sigma}$  with  $\boldsymbol{\sigma}$  being the Cauchy stress tensor and  $J = \det \mathbf{F}$ ). Consider a special case of elastic deformation where  $\dot{\mathbf{C}}^{vp} = 0$ ,  $\dot{\gamma}_i = 0$ , and  $\dot{r} = 0$ . Here Eq. (12) degenerates to

$$\left( \boldsymbol{\tau} - 2 \frac{\partial \Psi}{\partial \mathbf{b}^{ve}} \cdot \mathbf{b}^{ve} \right) : \mathbf{d} \geq 0. \quad (13)$$

Noting that Eq. (13) holds for arbitrarily chosen  $\mathbf{d}$  gives

$$\boldsymbol{\tau} = 2 \frac{\partial \Psi}{\partial \mathbf{b}^{ve}} \cdot \mathbf{b}^{ve} = 2 \frac{\partial \Psi_{ve}}{\partial \mathbf{b}^{ve}} \cdot \mathbf{b}^{ve}. \quad (14)$$

Define the following thermodynamic driving forces:

$$\mathbf{q}_i = -\frac{\partial \Psi}{\partial \gamma_i} = -\frac{\partial \Psi_{ve}}{\partial \gamma_i} \quad \text{and} \quad R = \frac{\partial \Psi}{\partial r} = \frac{d\Psi_{vp}}{dr}, \quad (15)$$

where  $\mathbf{q}_i$  is a stress measure conjugate to  $\gamma_i$ , and  $R$  is related to the current yield stress. Substituting Eqs. (14) and (15) into Eq. (12) gives

$$\Phi = \boldsymbol{\tau} : \left[ -\frac{1}{2} \mathcal{L}_v \mathbf{b}^{ve} \cdot (\mathbf{b}^{ve})^{-1} \right] + \sum_{i=1}^N \mathbf{q}_i : \dot{\gamma}_i - R\dot{r} \geq 0. \quad (16)$$

Also assume that  $\Phi$  can be decomposed into its viscoelastic and viscoplastic parts, i.e.,

$$\Phi = \Phi_{ve} + \Phi_{vp}, \quad (17)$$

where

$$\Phi_{ve} = \sum_{i=1}^N \mathbf{q}_i : \dot{\gamma}_i \geq 0 \quad \text{and} \quad \Phi_{vp} = \boldsymbol{\tau} : \left[ -\frac{1}{2} \mathcal{L}_v \mathbf{b}^{ve} \cdot (\mathbf{b}^{ve})^{-1} \right] - R \dot{r} \geq 0. \quad (18)$$

Following Ref. [12], assume that there is a viscoplastic potential, say  $\Omega$ , governing the evolution of  $\mathbf{b}^{ve}$  and  $r$ , such that

$$-\frac{1}{2} \mathcal{L}_v \mathbf{b}^{ve} \cdot (\mathbf{b}^{ve})^{-1} = \frac{\partial \Omega}{\partial \boldsymbol{\tau}} \quad \text{and} \quad \dot{r} = -\frac{\partial \Omega}{\partial R}. \quad (19)$$

Further assume that  $\Omega$  depends on  $\boldsymbol{\tau}$  and  $R$  via a yield function,  $f$ , such that

$$\Omega = \Omega(f) \quad \text{and} \quad \dot{v} = \frac{\partial \Omega}{\partial f}, \quad (20)$$

where  $\dot{v}$  is referred to as the viscosity function. Choosing a viscoplasticity model is then the equivalence of choosing  $f$  and  $\dot{v}$ . Combining Eqs. (19) and (20) gives the associated viscoplastic evolution laws as

$$\mathcal{L}_v \mathbf{b}^{ve} = -2\dot{v} \frac{\partial f}{\partial \boldsymbol{\tau}} \cdot \mathbf{b}^{ve} \quad \text{and} \quad \dot{r} = -\dot{v} \frac{\partial f}{\partial R}. \quad (21)$$

Polymers often exhibit non-associated viscoplastic flow. Assume that there exist a pseudo-plastic potential,  $F$ , such that the non-associated viscoplastic evolution laws read

$$\mathcal{L}_v \mathbf{b}^{ve} = -2\dot{v} \frac{\partial F}{\partial \boldsymbol{\tau}} \cdot \mathbf{b}^{ve} \quad \text{and} \quad \dot{r} = -\dot{v} \frac{\partial F}{\partial R}, \quad (22)$$

where  $\dot{v}$  is still given by Eq. (20). According to Ref. [12],  $\Omega$  has to be a convex function of  $\boldsymbol{\tau}$  and  $R$ , and so do  $f$  and  $F$ .

### III. General Radial Return

In this section, the general radial return algorithm in Ref. [5] is modified to accommodate the current objective. Suppose that all variables at a given instant of time,  $t_n$ , are known. Let  $(\cdot)_n$  denote a quantity at  $t_n$ , and let  $\Delta(\cdot) = (\cdot)_{n+1} - (\cdot)_n$ , e.g.,  $t_{n+1} = t_n + \Delta t$ . Let  $\Delta \mathbf{u}$  be prescribed displacement increments superposed upon spatial configuration  $\mathbf{x} = \mathbf{x}_n$  over  $[t_n, t_{n+1}]$ . For notational convenience, omit the subscript  $n+1$  on each quantity at  $t_{n+1}$ . Define relative deformation gradient<sup>5</sup>

$$\mathbf{f} = \mathbf{I} + \frac{\partial \mathbf{u}}{\partial \mathbf{x}} \quad (23)$$

such that  $\mathbf{F}$  can be related to  $\mathbf{F}_n$  by

$$\mathbf{F} = \mathbf{f} \cdot \mathbf{F}_n. \quad (24)$$

The evolution laws over  $[t_n, t_{n+1}]$  then read

$$\dot{\mathbf{f}} = \mathbf{l} \cdot \mathbf{f}, \quad \dot{\mathbf{b}}^{ve} = \mathbf{l} \cdot \mathbf{b}^{ve} + \mathbf{b}^{ve} \cdot \mathbf{l} - 2\dot{v} \frac{\partial F}{\partial \boldsymbol{\tau}}, \quad \dot{r} = -\dot{v} \frac{\partial F}{\partial R}. \quad (25)$$

Since  $\mathbf{u}$  and therefore  $\mathbf{f}$  are prescribed, the task is to find the other variables at  $t_{n+1}$ .

Here a radial return algorithm consists of the following steps:

1. trial viscoelastic step—assume that the deformation is entirely viscoelastic, apply so-called trial viscoelastic strains to the material, and compute the corresponding trial stresses
2. radial return step—reduce the trial strains along the viscoplastic flow direction such that the reduced strains and the resulting hardening variable(s) satisfy all constraints imposed by the viscoplasticity model

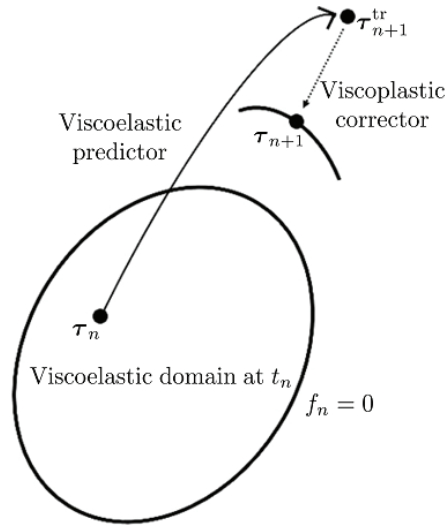


Figure 2. Radial return over  $[t_n, t_{n+1}]$ .

These steps are iterated to convergence (see Figure 2).

In the trial viscoelastic step,  $\dot{v} = 0$ , and Eq. (25) degenerates to

$$\dot{\mathbf{f}} = \mathbf{l} \cdot \mathbf{f}, \quad \dot{\mathbf{b}}^{ve} = \mathbf{l} \cdot \mathbf{b}^{ve} + \mathbf{b}^{ve} \cdot \mathbf{l}, \quad \dot{r} = 0. \quad (26)$$

Following Eq. (5), define the trial value of  $\mathbf{b}^{ve}$ , say  $(\mathbf{b}^{ve})^{\text{tr}}$ , as

$$(\mathbf{b}^{ve})^{\text{tr}} = \mathbf{f} \cdot \mathbf{F}_n^{ve} \cdot (\mathbf{f} \cdot \mathbf{F}_n^{ve})^T = \mathbf{f} \cdot \left[ \mathbf{F}_n^{ve} \cdot (\mathbf{F}_n^{ve})^T \right] \cdot \mathbf{f}^T = \mathbf{f} \cdot \mathbf{b}_n^{ve} \cdot \mathbf{f}^T. \quad (27)$$

Once the viscoelasticity model and  $(\mathbf{b}^{ve})^{\text{tr}}$  are specified, the trial stresses, say  $\boldsymbol{\tau}^{\text{tr}}$ , can be uniquely determined (see Section V for example).

In the radial return step, the evolution laws can be obtained by subtracting Eq. (26) from Eq. (25), i.e.,

$$\dot{\mathbf{f}} = \mathbf{0}, \quad \dot{\mathbf{b}}^{ve} = -2\dot{v} \frac{\partial \mathbf{F}}{\partial \boldsymbol{\tau}} \cdot \mathbf{b}^{ve}, \quad \dot{r} = -\dot{v} \frac{\partial \mathbf{F}}{\partial R}. \quad (28)$$

Suppose that  $\dot{v}$  remains constant in this step.  $\Delta v$  can then be related to  $\dot{v}$  using the backward Euler method by

$$\Delta v = \dot{v} \Delta t. \quad (29)$$

The second equation of Eq. (28) then becomes an ordinary differential equation over  $[t_n, t_{n+1}]$ , whose solution reads

$$\mathbf{b}^{ve} = \exp\left(-2\Delta v \frac{\partial \mathbf{F}}{\partial \boldsymbol{\tau}}\right) \cdot (\mathbf{b}^{ve})^{\text{tr}} \quad (30)$$

with  $(\mathbf{b}^{ve})^{\text{tr}}$  being the initial value of  $\mathbf{b}^{ve}$  in this step.  $r$  can then be updated as

$$r = r_n - \Delta v \frac{\partial \mathbf{F}}{\partial R}. \quad (31)$$

Assume that the material exhibits both elastic and plastic isotropy.  $\mathbf{b}^{ve}$  and  $\boldsymbol{\tau}$  then have the same principal directions and can be decomposed as

$$\mathbf{b}^{ve} = \sum_{A=1}^3 (\lambda_A^{ve})^2 \mathbf{p}_A \otimes \mathbf{p}_A \quad \text{and} \quad \boldsymbol{\tau} = \sum_{A=1}^3 \tau_A \mathbf{p}_A \otimes \mathbf{p}_A, \quad (32)$$

respectively, where  $\mathbf{p}_A$  denotes the  $A^{\text{th}}$  principal unit vector of  $\boldsymbol{\tau}$  and  $\mathbf{b}^{ve}$ ,  $\lambda_A^{ve}$  the  $A^{\text{th}}$  principal viscoelastic stretch, and  $\tau_A = \mathbf{p}_A \cdot \boldsymbol{\tau} \cdot \mathbf{p}_A$  the  $A^{\text{th}}$  eigenvalue of  $\boldsymbol{\tau}$ . The viscoelastic logarithmic strain tensor can then be

defined as

$$\boldsymbol{\epsilon}^{ve} = \sum_{A=1}^3 \epsilon_A^{ve} \mathbf{p}_A \otimes \mathbf{p}_A = \sum_{A=1}^3 \ln \lambda_A^{ve} \mathbf{p}_A \otimes \mathbf{p}_A. \quad (33)$$

$\Psi_{ve}$  can then be expressed as a function of  $\boldsymbol{\epsilon}^{ve}$  and  $\gamma_i$ 's, i.e.,

$$\Psi_{ve}(\boldsymbol{\epsilon}^{ve}, \gamma_1, \dots, \gamma_N) = \hat{\Psi}_{ve}(\boldsymbol{\epsilon}^{ve}, \gamma_1, \dots, \gamma_N), \quad (34)$$

such that

$$\boldsymbol{\tau} = \frac{\partial \hat{\Psi}_{ve}}{\partial \boldsymbol{\epsilon}^{ve}} \quad \text{and} \quad \mathbf{q}_i = -\frac{\partial \hat{\Psi}_{ve}}{\partial \gamma_i}. \quad (35)$$

$f$  and  $F$  can be treated as functions of  $\tau_A$ 's and  $R$ , i.e.,

$$f(\boldsymbol{\tau}, R) = \hat{f}(\tau_1, \tau_2, \tau_3, R) \quad \text{and} \quad F(\boldsymbol{\tau}, R) = \hat{F}(\tau_1, \tau_2, \tau_3, R). \quad (36)$$

For brevity, here only consider  $F$  and  $\hat{F}$ — $f$  and  $\hat{f}$  can be similarly analyzed. The following can be verified:

$$\frac{\partial F}{\partial \boldsymbol{\tau}} = \sum_{A=1}^3 \frac{\partial \hat{F}}{\partial \tau_A} \mathbf{p}_A \otimes \mathbf{p}_A. \quad (37)$$

First,  $(\boldsymbol{\epsilon}^{ve})^{\text{tr}}$  can be decomposed similarly to Eq. (32) as

$$(\boldsymbol{\epsilon}^{ve})^{\text{tr}} = \sum_{A=1}^3 \left[ (\lambda_A^{ve})^{\text{tr}} \right]^2 \mathbf{p}_A^{\text{tr}} \otimes \mathbf{p}_A^{\text{tr}}. \quad (38)$$

Second, the following can be obtained from Eq. (30):

$$(\boldsymbol{\epsilon}^{ve})^{\text{tr}} = \sum_{A=1}^3 (\lambda_A^{ve})^2 \exp\left(2\Delta v \frac{\partial \hat{F}}{\partial \tau_A}\right) \mathbf{p}_A \otimes \mathbf{p}_A. \quad (39)$$

Comparing Eq. (38) with Eq. (39) gives

$$\mathbf{p}_A = \mathbf{p}_A^{\text{tr}} \quad \text{and} \quad (\lambda_A^{ve})^2 = \exp\left(-2\Delta v \frac{\partial \hat{F}}{\partial \tau_A}\right) \left[ (\lambda_A^{ve})^{\text{tr}} \right]^2. \quad (40)$$

Taking the logarithm of both sides of the second equation of Eq (40) and combining the equation with Eq. (31) give

$$\boldsymbol{\epsilon}^{ve} = (\boldsymbol{\epsilon}^{ve})^{\text{tr}} - \Delta v \frac{\partial F}{\partial \boldsymbol{\tau}} \quad \text{and} \quad r = r_n - \Delta v \frac{\partial F}{\partial R}, \quad (41)$$

which are the evolution laws to be used hereafter.

#### IV. Viscoelasticity and Viscoplasticity Models

Choose a generalized Maxwell model containing  $N + 1$  springs and  $N$  dashpots (see Figure 13 for the 1D case) as the viscoelasticity model. The 3D model can be developed similarly to the 1D one in Appendix A. Let

$$\boldsymbol{\mathcal{E}}_i = K_i \mathbf{I} \otimes \mathbf{I} + 2G_i \boldsymbol{\mathcal{I}}' \quad (42)$$

be the fourth-order elasticity tensor of the  $i^{\text{th}}$  spring ( $i = 0, 1, \dots, N$ ), where  $K_i$  and  $G_i$  denotes the bulk and the shear spring moduli, respectively, and  $\boldsymbol{\mathcal{I}}' = \boldsymbol{\mathcal{I}} - \frac{1}{3} \mathbf{I} \otimes \mathbf{I}$  is the fourth-order deviatoric projection operator with  $\boldsymbol{\mathcal{I}}$  denoting the fourth-order identity tensor.  $\hat{\Psi}_{ve}$  can be expressed as the sum of its  $N + 1$  parts each of which represents a branch, i.e.,

$$\hat{\Psi}_{ve}(\boldsymbol{\epsilon}^{ve}, \gamma_1, \dots, \gamma_N) = \hat{\Psi}_0(\boldsymbol{\epsilon}^{ve}) + \sum_{i=1}^N \hat{\Psi}_i(\boldsymbol{\epsilon}^{ve}, \gamma_i), \quad (43)$$

where

$$\hat{\Psi}_0(\boldsymbol{\epsilon}^{ve}) = \frac{1}{2} \boldsymbol{\epsilon}^{ve} : \boldsymbol{\mathcal{E}}_0 : \boldsymbol{\epsilon}^{ve} \quad \text{and} \quad \hat{\Psi}_i(\boldsymbol{\epsilon}^{ve}, \gamma_i) = \frac{1}{2} (\boldsymbol{\epsilon}^{ve} - \boldsymbol{\gamma}_i) : \boldsymbol{\mathcal{E}}_i : (\boldsymbol{\epsilon}^{ve} - \boldsymbol{\gamma}_i) \quad (44)$$

are the zeroth and the  $i^{\text{th}}$  spring viscoelastic potentials, respectively. Substituting Eq. (43) into Eq. (35) gives

$$\boldsymbol{\tau} = \frac{d\hat{\Psi}_0}{d\boldsymbol{\epsilon}^{ve}} + \sum_{i=1}^N \frac{\partial \hat{\Psi}_i}{\partial \boldsymbol{\epsilon}^{ve}} \quad \text{and} \quad \mathbf{q}_i = -\frac{\partial \hat{\Psi}_i}{\partial \boldsymbol{\gamma}_i}. \quad (45)$$

Combining Eqs. (44) and (45) gives

$$\boldsymbol{\tau} = \boldsymbol{\tau}_0 + \sum_{i=1}^N \mathbf{q}_i, \quad (46)$$

where

$$\boldsymbol{\tau}_0 = \boldsymbol{\mathcal{E}}_0 : \boldsymbol{\epsilon}^{ve}, \quad (47)$$

and  $\mathbf{q}_i$ 's are to be determined. Let  $(\cdot)_m$  denote the mean of a second-order tensor, and let  $(\cdot)'$  denote the deviatoric part. Following Ref. [4], assume that  $(q_i)_m$  and  $\mathbf{q}'_i$  evolve independently such that

$$(\dot{q}_i)_m + \frac{(q_i)_m}{k_i} = 3K_i \dot{\boldsymbol{\epsilon}}_m^{ve} \quad \text{and} \quad \dot{\mathbf{q}}'_i + \frac{\mathbf{q}'_i}{g_i} = 2G_i \dot{\boldsymbol{\epsilon}}^{ve'}, \quad (48)$$

where  $k_i$  and  $g_i$  denote the volumetric and deviatoric characteristic relaxation times of the  $i^{\text{th}}$  branch, respectively. Solving Eq. (48) and noting that  $\mathbf{q} = 0$  at  $t = -\infty$  give

$$(q_i)_m = 3K_i \exp\left(-\frac{t}{k_i}\right) \int_{-\infty}^t \exp\left(\frac{s}{k_i}\right) \frac{\partial \boldsymbol{\epsilon}_m^{ve}}{\partial s} ds, \quad (49)$$

$$\mathbf{q}'_i = 2G_i \exp\left(-\frac{t}{g_i}\right) \int_{-\infty}^t \exp\left(\frac{s}{g_i}\right) \frac{\partial \boldsymbol{\epsilon}^{ve'}}{\partial s} ds. \quad (49')$$

Substituting Eq. (49) into Eq. (46) and rearrange the equation give

$$\tau_m = 3K_0 \boldsymbol{\epsilon}_m^{ve} + \sum_{i=1}^N 3K_i \exp\left(-\frac{t}{k_i}\right) \int_{-\infty}^t \exp\left(\frac{s}{k_i}\right) \frac{\partial \boldsymbol{\epsilon}_m^{ve}}{\partial s} ds, \quad (50)$$

$$\boldsymbol{\tau}' = 2G_0 \boldsymbol{\epsilon}^{ve'} + \sum_{i=1}^N 2G_i \exp\left(-\frac{t}{g_i}\right) \int_{-\infty}^t \exp\left(\frac{s}{g_i}\right) \frac{\partial \boldsymbol{\epsilon}^{ve'}}{\partial s} ds. \quad (50')$$

Let the material obey a yield function taking the general form of

$$f(\boldsymbol{\tau}, R) = g(\boldsymbol{\tau}) - \tau_y - R, \quad (51)$$

where  $g$  is a scalar-valued function to be specified, and  $\tau_y$  denotes the initial yield stress. Also let the material obey a pseudo-plastic potential taking the general form of

$$F(\boldsymbol{\tau}, R) = G(\boldsymbol{\tau}) - \tau_y - R, \quad (52)$$

where  $G$  is another scalar-valued function to be specified. If  $G(\boldsymbol{\tau}) = g(\boldsymbol{\tau})$ , the viscoplastic flow becomes associated, and Eq. (52) degenerates to Eq. (51). Also let

$$\mathbf{n} = \frac{\partial f}{\partial \boldsymbol{\tau}} = \frac{\partial g}{\partial \boldsymbol{\tau}} \quad \text{and} \quad \mathbf{N} = \frac{\partial F}{\partial \boldsymbol{\tau}} = \frac{\partial G}{\partial \boldsymbol{\tau}}. \quad (53)$$

Substituting Eq. (53) into Eq. (41) gives

$$\boldsymbol{\epsilon}^{ve} = (\boldsymbol{\epsilon}^{ve})^{\text{tr}} - \Delta v \mathbf{N} \quad \text{and} \quad \Delta r = r - r_n = \Delta v. \quad (54)$$

Eqs. (10) and (15) imply that  $R$  is a function of  $r$ , i.e.,  $R = R(r)$ .  $R = R(r)$  is referred to as the damage accumulation law, and its specific form is to be calibrated. Last set<sup>13</sup>

$$\dot{v} = \begin{cases} \gamma \left( \frac{f}{\tau_y + R} \right)^n & f \geq 0, \\ 0 & f < 0, \end{cases} \quad (55)$$

where  $\gamma$  denotes a viscosity parameter, and  $n$  denotes a rate-sensitivity parameter.

## V. Radial Return Algorithm

In this section, the viscoelasticity and the viscoplasticity models are implemented in the general radial return algorithm. Still consider time interval  $[t_n, t_{n+1}]$ .  $(q_m)_i$  and  $\mathbf{q}'_i$  can be related to  $[(q_m)_i]_n$  and  $(\mathbf{q}'_i)_n$  by

$$(q_m)_i = \exp\left(-\frac{\Delta t}{k_i}\right) [(q_m)_i]_n + 3K_i \exp\left(-\frac{t}{k_i}\right) \int_{t_n}^t \exp\left(\frac{s}{k_i}\right) \frac{\partial \epsilon_m^{ve}}{\partial s} ds, \quad (56)$$

$$\mathbf{q}'_i = \exp\left(-\frac{\Delta t}{g_i}\right) (\mathbf{q}'_i)_n + 2G_i \exp\left(-\frac{t}{g_i}\right) \int_{t_n}^t \exp\left(\frac{s}{g_i}\right) \frac{\partial \epsilon^{ve'}}{\partial s} ds, \quad (56')$$

respectively. Assume that  $\dot{\epsilon}^{ve}$  remains constant over  $[t_n, t]$ , and relate  $\Delta \epsilon^{ve}$  to  $\dot{\epsilon}^{ve}$  using the backward Euler method by

$$\Delta \epsilon^{ve} = \epsilon^{ve} - \epsilon_n^{ve} = \dot{\epsilon}^{ve} \Delta t. \quad (57)$$

Substituting Eq. (57) into Eq. (56) gives

$$(q_m)_i = \exp\left(-\frac{\Delta t}{k_i}\right) [(q_m)_i]_n + 3K_i \left[1 - \exp\left(-\frac{\Delta t}{k_i}\right)\right] \frac{k_i}{\Delta t} \Delta \epsilon_m^{ve}, \quad (58)$$

$$\mathbf{q}'_i = \exp\left(-\frac{\Delta t}{g_i}\right) (\mathbf{q}'_i)_n + 2G_i \left[1 - \exp\left(-\frac{\Delta t}{g_i}\right)\right] \frac{g_i}{\Delta t} \Delta \epsilon^{ve'}. \quad (58')$$

Substituting Eq. (58) into Eq. (56) gives

$$\tau_m = 3 \left(K_0 + \tilde{K}\right) \epsilon_m^{ve} + \sum_{i=1}^N \exp\left(-\frac{\Delta t}{k_i}\right) [(q_m)_i]_n - 3\tilde{K} (\epsilon_m^{ve})_n, \quad (59)$$

$$\boldsymbol{\tau}'_i = 2 \left(G_0 + \tilde{G}\right) \epsilon^{ve'} + \sum_{i=1}^N \exp\left(-\frac{\Delta t}{g_i}\right) (\mathbf{q}'_i)_n - 2\tilde{G} \epsilon_n^{ve'}, \quad (59')$$

where

$$\tilde{K} = \sum_{i=1}^N K_i \left[1 - \exp\left(-\frac{\Delta t}{k_i}\right)\right] \frac{k_i}{\Delta t} \quad \text{and} \quad \tilde{G} = \sum_{i=1}^N G_i \left[1 - \exp\left(-\frac{\Delta t}{g_i}\right)\right] \frac{g_i}{\Delta t}. \quad (60)$$

The trial stress tensor,  $\boldsymbol{\tau}^{\text{tr}}$ , can then be defined as

$$\boldsymbol{\tau}^{\text{tr}} = \left(\boldsymbol{\mathcal{E}}_0 + \tilde{\boldsymbol{\mathcal{E}}}\right) : (\boldsymbol{\epsilon}^{ve})^{\text{tr}} + \sum_{i=1}^N \left\{ \exp\left(-\frac{\Delta t}{k_i}\right) [(q_m)_i]_n \mathbf{I} + \exp\left(-\frac{\Delta t}{g_i}\right) (\mathbf{q}'_i)_n \right\} - \tilde{\boldsymbol{\mathcal{E}}} : \boldsymbol{\epsilon}_n^{ve}, \quad (61)$$

where

$$\tilde{\boldsymbol{\mathcal{E}}} = \tilde{K} \mathbf{I} \otimes \mathbf{I} + 2\tilde{G} \boldsymbol{\mathcal{I}}'. \quad (62)$$

The integration scheme can be formulated as solving the following equation set for  $\boldsymbol{\tau}$  and  $\Delta r$ :

$$\boldsymbol{\tau} = \boldsymbol{\tau}^{\text{tr}} - \Delta r \left(\boldsymbol{\mathcal{E}}_0 + \tilde{\boldsymbol{\mathcal{E}}}\right) : \mathbf{N}, \quad (63)$$

$$\Delta r = \dot{v} \Delta t. \quad (63')$$

The task can then be reformulated as solving the following equation set for  $\boldsymbol{\tau}$  and  $\Delta r$ :

$$\boldsymbol{\Psi}(\boldsymbol{\tau}, \Delta r) = \boldsymbol{\tau} - \boldsymbol{\tau}^{\text{tr}} + \Delta r \left(\boldsymbol{\mathcal{E}}_0 + \tilde{\boldsymbol{\mathcal{E}}}\right) : \mathbf{N} = \mathbf{0}, \quad (64)$$

$$P(\boldsymbol{\tau}, \Delta r) = \Delta r - \dot{v} \Delta t = 0. \quad (65)$$

Here Newton's method is used to obtain the solution. Require

$$\boldsymbol{\Psi}(\boldsymbol{\tau}_{\text{old}} + d\boldsymbol{\tau}, \Delta r_{\text{old}} + d\Delta r) = \boldsymbol{\Psi}(\boldsymbol{\tau}_{\text{old}}, \Delta r_{\text{old}}) + \frac{\partial \boldsymbol{\Psi}}{\partial \boldsymbol{\tau}} : d\boldsymbol{\tau} + \frac{\partial \boldsymbol{\Psi}}{\partial \Delta r} d\Delta r = \mathbf{0}, \quad (66)$$

$$P(\boldsymbol{\tau}_{\text{old}} + d\boldsymbol{\tau}, \Delta r_{\text{old}} + d\Delta r) = P(\boldsymbol{\tau}_{\text{old}}, \Delta r_{\text{old}}) + \frac{\partial P}{\partial \boldsymbol{\tau}} : d\boldsymbol{\tau} + \frac{\partial P}{\partial \Delta r} d\Delta r = 0, \quad (66')$$

where

$$\frac{\partial \Psi}{\partial \boldsymbol{\tau}} = \mathbf{I} + \Delta r \left( \boldsymbol{\varepsilon}_0 + \tilde{\boldsymbol{\varepsilon}} \right) : \frac{\partial \mathbf{N}}{\partial \boldsymbol{\tau}}, \quad \frac{\partial \Psi}{\partial \Delta r} = \left( \boldsymbol{\varepsilon}_0 + \tilde{\boldsymbol{\varepsilon}} \right) : \mathbf{N}, \quad (67)$$

$$\frac{\partial \mathbf{P}}{\partial \boldsymbol{\tau}} = -\frac{\partial \dot{v}}{\partial \boldsymbol{\tau}} \Delta t, \quad \frac{\partial \mathbf{P}}{\partial \Delta r} = 1 - \frac{\partial \dot{v}}{\partial \Delta r} \Delta t \quad (67')$$

with

$$\frac{\partial \dot{v}}{\partial \boldsymbol{\tau}} = n\gamma \left( \frac{g}{\tau_y + R} - 1 \right)^{n-1} \frac{\partial}{\partial \boldsymbol{\tau}} \left( \frac{g}{\tau_y + R} - 1 \right) = \frac{n\gamma}{\tau_y + R} \left( \frac{g}{\tau_y + R} - 1 \right)^{n-1} \mathbf{n}, \quad (68)$$

$$\frac{\partial \dot{v}}{\partial \Delta r} = n\gamma \left( \frac{g}{\tau_y + R} - 1 \right)^{n-1} \frac{\partial}{\partial \Delta r} \left( \frac{g}{\tau_y + R} - 1 \right) = -\frac{n\gamma g}{(\tau_y + R)^2} \left( \frac{g}{\tau_y + R} - 1 \right)^{n-1} \frac{dR}{d\Delta r}. \quad (68')$$

Note that, once  $g$  and  $G$  are specified,  $\mathbf{n}$ ,  $\mathbf{N}$ , and  $\partial \mathbf{N} / \partial \boldsymbol{\tau}$  can be uniquely determined (see Appendix B for example). Introduce matrix notation

$$\boldsymbol{\tau} = \left[ \begin{array}{cccccc} \tau_{11} & \tau_{12} & \tau_{22} & \tau_{13} & \tau_{23} & \tau_{33} \end{array} \right]^T. \quad (69)$$

Eq. (66) can be written in matrix form as

$$\left\{ \begin{array}{c} \Psi(\tau_{\text{old}}, \Delta r_{\text{old}}) \\ SP(\tau_{\text{old}}, \Delta r_{\text{old}}) \end{array} \right\} + J \left\{ \begin{array}{c} d\boldsymbol{\tau} \\ S d\Delta r \end{array} \right\} = 0, \quad (70)$$

where

$$J = \left[ \begin{array}{cc} \frac{\partial \Psi}{\partial \boldsymbol{\tau}} & \frac{1}{S} \frac{\partial \Psi}{\partial \Delta r} \\ S \frac{\partial \mathbf{P}}{\partial \boldsymbol{\tau}} & \frac{\partial \mathbf{P}}{\partial \Delta r} \end{array} \right] \quad (71)$$

is a  $7 \times 7$  Jacobian matrix, and  $S = dR/d\Delta r$  is a scale factor making  $J$  well-conditioned. Rearranging Eq. (70) gives

$$\left\{ \begin{array}{c} d\boldsymbol{\tau} \\ S d\Delta r \end{array} \right\} = -J^{-1} \left\{ \begin{array}{c} \Psi(\tau_{\text{old}}, \Delta r_{\text{old}}) \\ SP(\tau_{\text{old}}, \Delta r_{\text{old}}) \end{array} \right\}. \quad (72)$$

The corrections can then be computed and added to the solutions, i.e.,

$$\boldsymbol{\tau}_{\text{new}} = \boldsymbol{\tau}_{\text{old}} + d\boldsymbol{\tau} \quad \text{and} \quad \Delta r_{\text{new}} = \Delta r_{\text{old}} + d\Delta r. \quad (73)$$

This process is iterated to convergence.

## VI. Incremental Constitutive Relation

In this section, the incremental constitutive relation for the material is first derived in the spatial configuration and then pulled-back to the material configuration. It facilitates the implementation of the constitutive model in either an FE code or the variational homogenization method (see Section VII).

The incremental constitutive relation can be written as

$$d\mathbf{S} = \boldsymbol{\mathcal{C}} : \frac{1}{2} d\mathbf{C}, \quad (74)$$

where  $\mathbf{S}$  denotes the second Piola–Kirchhoff stress tensor, and

$$\boldsymbol{\mathcal{C}} = 2 \frac{\partial \mathbf{S}}{\partial \mathbf{C}} \quad (75)$$

is the fourth-order second elasticity tensor. The fourth-order spatial elasticity tensor,  $\boldsymbol{\mathcal{C}}^{\text{SP}}$ , can be obtained by pushing-forward  $\boldsymbol{\mathcal{C}}$  to the spatial configuration, i.e.,

$$\boldsymbol{\mathcal{C}}_{ijkl}^{\text{SP}} = J^{-1} F_{im} F_{jn} F_{kp} F_{lq} \boldsymbol{\mathcal{C}}_{mnpq} = 2J^{-1} F_{im} F_{jn} F_{kp} F_{lq} \frac{\partial S_{mn}}{\partial C_{pq}}. \quad (76)$$

The spatial representation of Eq. (74) then reads<sup>14</sup>

$$\mathcal{L}_v \boldsymbol{\tau} = \mathbf{J}\mathcal{C}^{\text{SP}} : \mathbf{d} \quad \text{or} \quad \dot{\boldsymbol{\tau}} = \mathbf{J}\mathcal{C}^{\text{SP}} : \mathbf{d} + \mathbf{l} \cdot \boldsymbol{\tau} + \boldsymbol{\tau} \cdot \mathbf{l}^T. \quad (77)$$

The task is to obtain the explicit expression for  $\mathcal{C}^{\text{SP}}$  from Eq. (76).

Eq. (32) can be rewritten as

$$\boldsymbol{\tau} = \sum_{A=1}^3 \tau_A \mathbf{q}_A, \quad \text{where} \quad \mathbf{q}_A = \mathbf{p}_A \otimes \mathbf{p}_A. \quad (78)$$

$\mathbf{S}$  can be related to  $\boldsymbol{\tau}$  by

$$\mathbf{S} = \mathbf{F}^{-1} \cdot \boldsymbol{\tau} \cdot \mathbf{F}^{-T}. \quad (79)$$

Substituting Eqs. (78) and (79) into Eq. (76) gives

$$\begin{aligned} \mathcal{C}_{ijkl}^{\text{SP}} &= 2J^{-1} F_{im} F_{jn} F_{kp} F_{lq} \frac{\partial}{\partial C_{pq}} \left[ \sum_{A=1}^3 \tau_A F_{mr}^{-1}(q_A)_{rs} F_{sn}^{-T} \right] \\ &= 2J^{-1} F_{im} F_{jn} F_{kp} F_{lq} \sum_{A=1}^3 F_{mr}^{-1}(q_A)_{rs} F_{sn}^{-T} \frac{\partial \tau_A}{\partial C_{pq}} \\ &\quad + 2J^{-1} F_{im} F_{jn} F_{kp} F_{lq} \sum_{A=1}^3 \tau_A \frac{\partial}{\partial C_{pq}} [F_{mr}^{-1}(q_A)_{rs} F_{sn}^{-T}]. \end{aligned} \quad (80)$$

Define the following fourth-order tensor:

$$\mathbf{c}^{\text{alg}} = \sum_{A=1}^3 \mathbf{q}_A \otimes \frac{\partial \tau_A}{\partial (\epsilon^{ve})^{\text{tr}}}, \quad (81)$$

which is actually the algorithmic tangent operator when  $\mathbf{p}_A$ 's are held fixed.  $\mathbf{c}^{\text{alg}}$  can be expressed as a  $3 \times 3$  matrix in principal stress space, whose components reads

$$\mathcal{C}_{AB}^{\text{alg}} = \frac{\partial \tau_A}{\partial (\epsilon^{ve})_B^{\text{tr}}}, \quad \text{where} \quad A, B = 1, 2, 3. \quad (82)$$

The following can be verified:

$$2\mathbf{F} \cdot \frac{\partial (\epsilon^{ve})_B^{\text{tr}}}{\partial \mathbf{C}} \cdot \mathbf{F}^T = \mathbf{q}_B \quad (83)$$

(see Appendix C for the derivation). With the help of Eqs. (82) and (83), the first term on the right side of Eq. (80) can further be expressed using the chain rule as

$$\begin{aligned} &2F_{im} F_{jn} F_{kp} F_{lq} \sum_{A=1}^3 F_{mr}^{-1}(q_A)_{rs} F_{sn}^{-T} \frac{\partial \tau_A}{\partial C_{pq}} \\ &= \sum_{A=1}^3 \sum_{B=1}^3 (q_A)_{ij} \frac{\partial \tau_A}{\partial (\epsilon^{ve})_B^{\text{tr}}} \left[ 2F_{kp} \frac{\partial (\epsilon^{ve})_B^{\text{tr}}}{\partial C_{pq}} F_{ql}^T \right] = \sum_{A=1}^3 \sum_{B=1}^3 \mathcal{C}_{AB}^{\text{alg}}(q_A)_{ij} (q_B)_{kl}. \end{aligned} \quad (84)$$

Define the following fourth-order tensor:

$$(\mathcal{R}_A)_{ijkl} = F_{im} F_{jn} F_{kp} F_{lq} \frac{\partial}{\partial C_{pq}} [F_{mr}^{-1}(q_A)_{rs} F_{sn}^{-T}], \quad (85)$$

whose explicit expression can be found in Appendix C. Substituting Eqs. (84) and (85) into Eq. (82) gives

$$\mathcal{C}^{\text{SP}} = J^{-1} \sum_{A=1}^3 \sum_{B=1}^3 \mathcal{C}_{AB}^{\text{alg}} \mathbf{q}_A \otimes \mathbf{q}_B + 2J^{-1} \sum_{A=1}^3 \tau_A \mathcal{R}_A, \quad (86)$$

where the explicit expression for  $\mathbf{C}^{\text{alg}}$  is to be derived.

Hereafter hold  $\mathbf{p}_A$ 's fixed. Totally differentiating both sides of Eq. (64) with respect to  $\boldsymbol{\tau}$ ,  $\Delta r$ , and  $(\boldsymbol{\epsilon}^{ve})^{\text{tr}}$  gives

$$d\Psi = \frac{\partial\Psi}{\partial\boldsymbol{\tau}} : d\boldsymbol{\tau} + \frac{\partial\Psi}{\partial\Delta r} d\Delta r + \frac{\partial\Psi}{\partial(\boldsymbol{\epsilon}^{ve})^{\text{tr}}} : d(\boldsymbol{\epsilon}^{ve})^{\text{tr}} = \mathbf{0}, \quad (87)$$

$$dP = \frac{\partial P}{\partial\boldsymbol{\tau}} : d\boldsymbol{\tau} + \frac{\partial P}{\partial\Delta r} d\Delta r + \frac{\partial P}{\partial(\boldsymbol{\epsilon}^{ve})^{\text{tr}}} : d(\boldsymbol{\epsilon}^{ve})^{\text{tr}} = 0, \quad (88)$$

where

$$\frac{\partial\Psi}{\partial(\boldsymbol{\epsilon}^{ve})^{\text{tr}}} = -\frac{\partial\boldsymbol{\tau}^{\text{tr}}}{\partial(\boldsymbol{\epsilon}^{ve})^{\text{tr}}} = -(\boldsymbol{\mathcal{E}}_0 + \tilde{\boldsymbol{\mathcal{E}}}) \quad \text{and} \quad \frac{\partial P}{\partial(\boldsymbol{\epsilon}^{ve})^{\text{tr}}} = 0. \quad (89)$$

Solving Eq. (92) for  $d\Delta r$  gives

$$d\Delta r = -\frac{\frac{\partial P}{\partial\boldsymbol{\tau}}}{\frac{\partial P}{\partial\Delta r}} : d\boldsymbol{\tau}. \quad (90)$$

Substituting Eq. (90) into Eq. (87) and solving the equation for  $d\boldsymbol{\tau}$  gives

$$d\boldsymbol{\tau} = \left( \frac{\partial\Psi}{\partial\boldsymbol{\tau}} - \frac{\frac{\partial\Psi}{\partial\Delta r} \otimes \frac{\partial P}{\partial\boldsymbol{\tau}}}{\frac{\partial P}{\partial\Delta r}} \right)^{-1} : (\boldsymbol{\mathcal{E}}_0 + \tilde{\boldsymbol{\mathcal{E}}}) : d(\boldsymbol{\epsilon}^{ve})^{\text{tr}} \equiv \mathbf{C}^{\text{alg}} : d(\boldsymbol{\epsilon}^{ve})^{\text{tr}}, \quad (91)$$

which gives the explicit expression for  $\mathbf{C}^{\text{alg}}$ .

An alternative form of Eq. (74) reads

$$\dot{\mathbf{P}} = \mathbf{A} : \dot{\mathbf{F}}. \quad (92)$$

where  $\mathbf{P}$  denotes the first Piola–Kirchhoff stress tensor, and

$$\mathbf{A} = \frac{\partial\mathbf{P}}{\partial\mathbf{F}} \quad (93)$$

is the fourth-order first elasticity tensor. According to Ref. [11], a variational statement formulated with Eq. (92) is preferred for homogenization. The tasks are then (1) relating  $\mathbf{C}$  to  $\mathbf{C}^{\text{sp}}$  and (2) relating  $\mathbf{A}$  to  $\mathbf{C}$ .  $\mathbf{C}$  can be obtained by pulling-back  $\mathbf{C}^{\text{sp}}$  to the material configuration, i.e.,

$$\mathcal{C}_{ijkl} = J F_{im}^{-1} F_{jn}^{-1} F_{kp}^{-1} F_{lq}^{-1} \mathcal{C}_{mnpq}^{\text{sp}}. \quad (94)$$

$\mathbf{P}$  can be related to  $\mathbf{S}$  by

$$\mathbf{P} = \mathbf{F} \cdot \mathbf{S}. \quad (95)$$

Combining Eqs. (75) and (92)–(95) gives

$$\mathbf{A} = \frac{\partial\mathbf{P}}{\partial\mathbf{F}} = \frac{\partial}{\partial\mathbf{F}} (\mathbf{F} \cdot \mathbf{S}) = \boldsymbol{\mathcal{I}} \cdot \mathbf{S} + \mathbf{F} \cdot \frac{\partial\mathbf{S}}{\partial\mathbf{F}} = \boldsymbol{\mathcal{I}} \cdot \mathbf{S} + \mathbf{F} \cdot \frac{\partial\mathbf{S}}{\partial\mathbf{C}} : \frac{\partial\mathbf{C}}{\partial\mathbf{F}} = \boldsymbol{\mathcal{I}} \cdot \mathbf{S} + \frac{1}{2} \mathbf{F} \cdot \mathbf{C} : \frac{\partial\mathbf{C}}{\partial\mathbf{F}}. \quad (96)$$

The first term to the right of the last equal sign in Eq. (96) can be expressed as

$$\mathcal{I}_{ijkm} S_{ml} = \delta_{ik} \delta_{jm} S_{ml} = \delta_{ik} S_{jl}, \quad (97)$$

and the second term

$$\begin{aligned} \frac{1}{2} F_{im} \mathcal{C}_{mjnp} \frac{\partial \mathcal{C}_{np}}{\partial F_{kl}} &= \frac{1}{2} F_{im} \mathcal{C}_{mjnp} \frac{\partial}{\partial F_{kl}} (F_{qn} F_{qp}) = \frac{1}{2} F_{im} \mathcal{C}_{mjnp} (F_{qn} \mathcal{I}_{qpkl} + F_{qp} \mathcal{I}_{qnkl}) \\ &= F_{im} \mathcal{C}_{jmnp} F_{qn} \mathcal{I}_{qpkl} = F_{im} \mathcal{C}_{mjnp} F_{qn} \delta_{qk} \delta_{pl} = F_{im} \mathcal{C}_{mjnl} F_{kn}. \end{aligned} \quad (98)$$

Note that the third equality in Eq. (98) holds because  $\mathbf{C}$  fulfills the minor symmetries. Substituting Eqs. (97) and (98) into Eq. (96) gives

$$\mathcal{A}_{ijkl} = \delta_{ik} S_{jl} + F_{im} \mathcal{C}_{mjnl} F_{kn}. \quad (99)$$

Once  $\mathbf{C}^{\text{sp}}$  is computed,  $\mathbf{A}$  can be obtained from  $\mathbf{C}^{\text{sp}}$  using Eq. (94) and (99).

## VII. Variational Asymptotic Homogenization

Consider a composite consisting of one or more constituents obeying the above incremental constitutive relation, and suppose that the composite has an identifiable SG. In this section, a variational statement of the SG is formulated. Introduce global coordinates  $\mathbf{X} = (X_1, X_2, X_3)$  describing the macroscopic structure, and introduce local coordinates  $\mathbf{Y} = (Y_1, Y_2, Y_3)$  describing the SG so that

$$\mathbf{Y} = \frac{\mathbf{X}}{\varepsilon}, \quad (100)$$

where  $\varepsilon \ll 1$  is a scale ratio. Suppose that all global and local variables at  $t_n$  are known. The task is to find the current displacements in the SG,  $u_i$ . The present approach is similar to the approach used in Ref. [11]. In Ref. [11], the variational statement is formulated with a strain energy density function relating  $\mathbf{P}$  to  $\mathbf{F}$ . The main difference herein is that the variational statement is formulated with a state function relating  $\dot{\mathbf{P}}$  to  $\dot{\mathbf{F}}$  (see Eq. (101)) because there is no one-to-one correspondence between  $\mathbf{P}$  and  $\mathbf{F}$ . To ensure the completeness of derivation, all necessary equations are presented in Sections VII and VIII.

Following Ref. [15], define a state function,  $W^*$ , as

$$W^* \left( \dot{F}_{ij} \right) = \frac{1}{2} \dot{F}_{ij} \mathcal{A}_{ijkl} \dot{F}_{kl} \quad (101)$$

so that

$$\delta W^* = \delta \dot{F}_{ij} \mathcal{A}_{ijkl} \dot{F}_{kl} = \dot{P}_{ij} \delta \dot{F}_{ij} \quad (102)$$

(see also Eq. (92), and see Figure 3 for the physical meaning of  $W^*$ ). It can be verified that, for  $\varepsilon \rightarrow 0$ , external forces negligibly contribute to the integral of  $W^*$  over the SG.<sup>6</sup> The following variational principle can then be created for viscoelastic-viscoplastic composites: among all admissible velocities, the actual velocities make functional

$$U^* = \int_{\Omega} W^* \left( \dot{F}_{ij} \right) dV \equiv \langle W^* \rangle, \quad (103)$$

an absolute minimum (see Ref. [15] for more details), i.e.,

$$\delta U^* = \left\langle \frac{\partial W^*}{\partial \dot{F}_{ij}} \delta \dot{F}_{ij} \right\rangle = \left\langle \dot{P}_{ij} \delta \frac{\partial u_i}{\partial X_j} \right\rangle = 0 \quad (104)$$

and

$$\delta^2 U^* = \left\langle \frac{\partial^2 W^*}{\partial \dot{F}_{ij} \partial \dot{F}_{kl}} \delta \dot{F}_{ij} \delta \dot{F}_{kl} \right\rangle = \left\langle \mathcal{A}_{ijkl} \delta \dot{F}_{ij} \delta \dot{F}_{kl} \right\rangle \geq 0, \quad (105)$$

where  $\Omega$  denotes the domain occupied by the SG (with boundary  $\partial\Omega$ ) and also its volume, and  $\langle \cdot \rangle$  denotes the integral of a quantity over  $\Omega$ . Note that the inequality in Eq. (105) holds because  $\mathcal{A}_{ijkl}$  is positive-definite.

Assume that

$$\dot{u}_i = \dot{u}_i(\mathbf{X}, \mathbf{Y}) \quad (106)$$

is a smooth function of  $\mathbf{X}$  and  $\mathbf{Y}$ . The derivatives of  $\dot{u}_i$  can be expressed as<sup>6</sup>

$$\frac{\partial \dot{u}_i}{\partial X_j} = \left( \frac{\partial \dot{u}_i}{\partial X_j} \right)_{\mathbf{Y}} + \frac{1}{\varepsilon} \left( \frac{\partial \dot{u}_i}{\partial Y_j} \right)_{\mathbf{X}} \equiv \dot{u}_{i,j} + \frac{1}{\varepsilon} \dot{u}_{i|j}. \quad (107)$$

Substituting Eq. (107) into Eq. (104) gives

$$\delta U^* = \left\langle \frac{\partial U^*}{\partial \dot{F}_{ij}} \delta \dot{F}_{ij} \right\rangle = \left\langle \dot{P}_{ij} \delta (u_{i,j}) + \dot{P}_{ij} \delta \left( \frac{1}{\varepsilon} \dot{u}_{i|j} \right) \right\rangle = \left\langle \dot{P}_{ij} \delta \left( \frac{1}{\varepsilon} \dot{u}_{i|j} \right) \right\rangle = 0, \quad (108)$$

where the third equality holds because the omitted term negligibly contributes to  $\delta U^*$  ( $\varepsilon \ll 1$ ). Eq. (108) has solution

$$\dot{u}_i(\mathbf{X}, \mathbf{Y}) = \dot{\bar{u}}_i(\mathbf{X}). \quad (109)$$

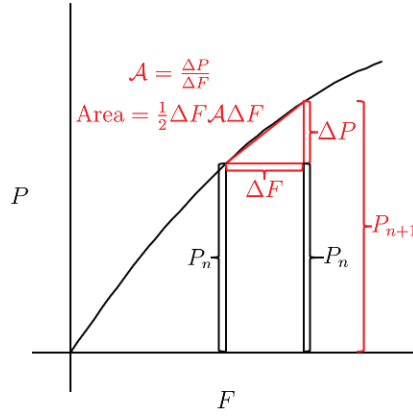


Figure 3. 1D example over  $[t_n, t_{n+1}]$ .  $P_n$  is known, and quantities in red are of interest.  $A = \frac{\Delta P}{\Delta F}$  thanks to linearization. Given the quantities related to the red triangle,  $P_{n+1}$  and the other quantities at  $t_{n+1}$  can be obtained subsequently. Since  $\Delta F = \dot{F}\Delta t$ , here state function  $W^*$  times  $(\Delta t)^2$  equals the area of the red triangle.

Eqs. (108) and (109) imply that  $\dot{u}_i(\mathbf{X}, \mathbf{Y})$  should be a rapidly oscillatory function not significantly deviating from slowly varying function  $\dot{u}_i(\mathbf{X})$ .  $\dot{u}_i$  can then be asymptotically expanded into the sum of  $\dot{u}_i$  and a fluctuation function, say  $\dot{\chi}_i$ , i.e.,

$$\dot{u}_i(\mathbf{X}, \mathbf{Y}) = \dot{u}_i(\mathbf{X}) + \varepsilon \dot{\chi}_i(\mathbf{X}, \mathbf{Y}), \quad (110)$$

where  $\dot{\chi}_i$  should be a periodic function of  $\mathbf{Y}$  and may also depend on  $\mathbf{X}$ , and  $\varepsilon \dot{\chi}_i$  is asymptotically smaller than  $\dot{u}_i$ . Require

$$\frac{1}{\Omega} \int_{\Omega} \dot{\chi}_i dV \equiv \langle \dot{\chi}_i \rangle = 0 \quad (111)$$

so that

$$\dot{u}_i = \langle \dot{u}_i \rangle \quad (112)$$

becomes the global displacement vector,<sup>6</sup> where  $\langle \langle \cdot \rangle \rangle$  denotes the average of a quantity over  $\Omega$ . Substituting Eq. (110) into Eq. (107) gives

$$\frac{\partial \dot{u}_i}{\partial X_j} = \frac{\partial \dot{u}_i}{\partial X_j} + \varepsilon \dot{\chi}_{i,j} + \dot{\chi}_{i|j}. \quad (113)$$

It can be similarly verified that  $\varepsilon \dot{\chi}_{i,j}$  negligibly affects Eq. (104) and is therefore omissible. Let

$$\bar{F}_{ij} = \delta_{ij} + \frac{\partial \dot{u}_i}{\partial X_j}, \quad (114)$$

which actually denotes the global deformation gradient tensor. Combining Eqs. (2), (113), and (114) gives

$$F_{ij} = \bar{F}_{ij} + \chi_{i|j}. \quad (115)$$

Next hold  $\dot{\bar{F}}_{ij}$  fixed. With Eq. (115), the above variational principle can be revised as follows: among all admissible fluctuation functions, the actual fluctuation functions make functional  $U^*$  an absolute minimum, i.e.,

$$\delta U^* = \left\langle \frac{\partial W^*}{\partial \dot{F}_{ij}} \delta \dot{F}_{ij} \right\rangle = \langle \dot{P}_{ij} \delta \dot{\chi}_{i|j} \rangle = 0, \quad (116)$$

which is the variational statement to be solved in Section VIII.

## VIII. FE Implementation

In this section, the above variational statement is first discretized in a finite-dimensional space and then solved using an Euler–Newton predictor–corrector method. Introduce the following matrix notations:

$$\bar{F} = \left[ \begin{array}{ccccccccc} \bar{F}_{11} & \bar{F}_{12} & \bar{F}_{22} & \bar{F}_{13} & \bar{F}_{23} & \bar{F}_{33} & \bar{F}_{21} & \bar{F}_{31} & \bar{F}_{32} \end{array} \right]^T, \quad (117)$$

$$\left\{ \begin{array}{c} \frac{\partial \chi_1}{\partial Y_1} \\ \frac{\partial \chi_1}{\partial Y_2} \\ \frac{\partial \chi_2}{\partial Y_2} \\ \frac{\partial \chi_1}{\partial Y_3} \\ \frac{\partial \chi_2}{\partial Y_3} \\ \frac{\partial \chi_3}{\partial Y_3} \\ \frac{\partial \chi_2}{\partial Y_1} \\ \frac{\partial \chi_3}{\partial Y_1} \\ \frac{\partial \chi_3}{\partial Y_2} \end{array} \right\} = \left[ \begin{array}{ccc} \frac{\partial}{\partial Y_1} & 0 & 0 \\ \frac{\partial}{\partial Y_2} & 0 & 0 \\ 0 & \frac{\partial}{\partial Y_2} & 0 \\ \frac{\partial}{\partial Y_3} & 0 & 0 \\ 0 & \frac{\partial}{\partial Y_3} & 0 \\ 0 & 0 & \frac{\partial}{\partial Y_3} \\ 0 & \frac{\partial}{\partial Y_1} & 0 \\ 0 & 0 & \frac{\partial}{\partial Y_1} \\ 0 & 0 & \frac{\partial}{\partial Y_2} \end{array} \right] \left\{ \begin{array}{c} \chi_1 \\ \chi_2 \\ \chi_3 \end{array} \right\} \equiv \Gamma_h \chi, \quad (117')$$

where  $\Gamma_h$  denotes an operator matrix, and  $\chi$  denotes a column matrix containing the components of the fluctuation function. Let  $\chi$  be discretized in a finite-dimensional space as

$$\chi(X_i, Y_i) = S(Y_i) \mathcal{X}(X_i), \quad (118)$$

where  $S$  denotes the shape function, and  $\mathcal{X}$  denotes a column matrix containing the nodal values of the fluctuation function at all active nodes. Eq. (115) can be discretized as

$$F = \bar{F} + \Gamma_h S \mathcal{X}. \quad (119)$$

The task then becomes finding  $\bar{F}$  and  $\mathcal{X}$ . Here a multilevel Newton method<sup>16</sup> is used for problem solving due to the following reasons:

- $\bar{F}$  and  $\mathcal{X}$  are implicitly linked, making it numerically prohibitive to solve for them simultaneously.
- This method fits a multiscale simulation well.

The multilevel Newton method is not guaranteed to converge to the solution and often gets “lost” if started far from the solution. Fortunately, it can be embedded in an Euler–Newton predictor–corrector method<sup>17</sup> for improved convergence. This method consists of the following steps:

1. Euler predictor step—proceed in the tangent direction of the loading path
2. Newton corrector step—bring the predictions back to the loading path

In the remaining of this section, the details on these steps will be presented in succession.

### A. Euler Predictor Step

Suppose that all global and local variables at a given instant of time are known. Note that such derivative of a quantity can be converted to its corresponding increment by multiplying it by the time increment,  $\Delta t$ . The task can then be reformulated as finding the current velocities in the SG,  $\dot{u}_i$ . Eq. (103) can be discretized as

$$U^* = \frac{1}{2} \left( \dot{\chi}^T D_{hh} \dot{\chi} + 2 \dot{\chi}^T D_{hF} \dot{\bar{F}} + \dot{\bar{F}}^T D_{FF} \dot{\bar{F}} \right), \quad (120)$$

where

$$D_{hh} = \left\langle (\Gamma_h S)^T D (\Gamma_h S) \right\rangle, \quad D_{hF} = \left\langle (\Gamma_h S)^T D \right\rangle, \quad D_{FF} = \langle D \rangle. \quad (121)$$

$U^*$  attains its minimum if and only if

$$D_{hh} \dot{\chi} = -D_{hF} \dot{\bar{F}} \quad \text{or} \quad \dot{\chi} = \chi_0 \dot{\bar{F}}, \quad (122)$$

which implies that  $\dot{\mathcal{X}}$  linearly depends on  $\dot{\bar{F}}$ . Substituting Eq. (122) into Eq. (120) gives

$$U^* = \frac{1}{2} \dot{\bar{F}}^T (\mathcal{X}_0^T D_{hF} + D_{FF}) \dot{\bar{F}} \equiv \frac{\Omega}{2} \dot{\bar{F}}^T \bar{D} \dot{\bar{F}}, \quad (123)$$

where  $\bar{D}$  denotes the effective tangent stiffness matrix. Let  $\bar{P}$  denote the global first Piola–Kirchhoff stress column matrix. By definition,

$$\dot{\bar{P}} = \frac{\partial}{\partial \dot{\bar{F}}} \langle \langle W^* \rangle \rangle = \bar{D} \dot{\bar{F}}. \quad (124)$$

Eq. (124) can be partitioned as

$$\begin{Bmatrix} \dot{\bar{P}}_u \\ \dot{\bar{P}}_k \end{Bmatrix} = \begin{bmatrix} \bar{D}_{uk} & \bar{D}_{uu} \\ \bar{D}_{kk} & \bar{D}_{ku} \end{bmatrix} \begin{Bmatrix} \dot{\bar{F}}_k \\ \dot{\bar{F}}_u \end{Bmatrix}, \quad (125)$$

where the subscripts  $k$  and  $u$  denote the known and the unknown components, respectively. In Eq. (125),  $\dot{\bar{P}}_u$  and  $\dot{\bar{F}}_u$  need to be determined. Rearranging Eq. (125) gives

$$\begin{Bmatrix} \dot{\bar{P}}_u \\ \dot{\bar{F}}_u \end{Bmatrix} = \begin{bmatrix} \bar{D}_{uk} - \bar{D}_{uu} \bar{D}_{ku}^{-1} \bar{D}_{kk} & \bar{D}_{uu} \bar{D}_{ku}^{-1} \\ -\bar{D}_{ku}^{-1} \bar{D}_{kk} & \bar{D}_{ku}^{-1} \end{bmatrix} \begin{Bmatrix} \dot{\bar{F}}_k \\ \dot{\bar{P}}_k \end{Bmatrix}, \quad (126)$$

from which  $\dot{\bar{P}}_u$  and  $\dot{\bar{F}}_u$  can be determined (and so can the global response of the SG). After this, the local deformation gradient rates can be obtained as

$$\dot{F} = \dot{\bar{F}} + \Gamma_h S \mathcal{X}_0 \dot{\bar{F}}. \quad (127)$$

## B. Newton Corrector Step

The multilevel Newton method consists of the following loops:

- inner loop— $\bar{F}$  is held fixed, and  $\mathcal{X}$  is the variable
- outer loop— $\mathcal{X}$  is held fixed, and the unknown components of  $\bar{P}$  and  $\bar{F}$  (i.e.,  $\bar{P}_u$  and  $\bar{F}_u$ ) are the variables

Note that, if  $\bar{F}$  is fully prescribed (this is usually the case in multiscale simulations), only the inner loop is needed. First consider the inner loop. The incremental form of Eq. (116) is given by

$$\delta U^* = \langle \Delta P_{ij} \delta (\Delta \chi_{ij}) \rangle = 0 \quad (128)$$

or

$$\delta U^* = \left\langle \left[ P_{ij} - (P_n)_{ij} \right] \delta \left[ \chi_{ij} - (\chi_n)_{ij} \right] \right\rangle = \left\langle \left[ P_{ij} - (P_n)_{ij} \right] \delta \chi_{ij} \right\rangle = 0. \quad (129)$$

Eq. (129) can be discretized as

$$\delta U^* = \delta \mathcal{X}^T \left\langle (\Gamma_h S)^T [P(\mathcal{X}) - P_n] \right\rangle = 0, \quad (130)$$

where  $P$  denotes the local first Piola–Kirchhoff stress column matrix. The second equality in Eq. (130) holds only if

$$\Psi_{\text{in}}(\mathcal{X}) = \left\langle (\Gamma_h S)^T [P(\mathcal{X}) - P_n] \right\rangle = 0. \quad (131)$$

Suppose that Eq. (131) is zeroed in each previous step. This implies that

$$\left\langle (\Gamma_h S)^T P_n \right\rangle = 0. \quad (132)$$

Substituting Eq. (132) into Eq. (131) gives

$$\Psi_{\text{in}}(\mathcal{X}) = \left\langle (\Gamma_h S)^T P(\mathcal{X}) \right\rangle = 0. \quad (133)$$

The task of the inner loop is therefore to solve Eq. (133) (rather than Eq. (131) to eliminate the accumulation of errors) for  $\mathcal{X}$ . Require

$$\Psi_{\text{in}}(\mathcal{X}_{\text{old}} + d\mathcal{X}) = \Psi_{\text{in}}(\mathcal{X}_{\text{old}}) + \frac{\partial \Psi_{\text{in}}}{\partial \mathcal{X}} d\mathcal{X} = 0. \quad (134)$$

Solving Eq. (134) for the corrections,  $d\mathcal{X}$ , gives

$$\frac{\partial \Psi_{\text{in}}}{\partial \mathcal{X}} d\mathcal{X} = -\Psi_{\text{in}}(\mathcal{X}_{\text{old}}), \quad (135)$$

where

$$\frac{\partial \Psi_{\text{in}}}{\partial \mathcal{X}} = \left\langle (\Gamma_h S)^T \frac{\partial P}{\partial \mathcal{X}} \right\rangle = \left\langle (\Gamma_h S)^T D (\Gamma_h S) \right\rangle \equiv D_{hh} \quad (136)$$

with  $D$  denoting the  $9 \times 9$  tangent stiffness matrix condensed from  $\mathcal{A}$ , using Voigt notation. The corrections can then be computed and added to the solution, i.e.,

$$\mathcal{X}_{\text{new}} = \mathcal{X}_{\text{old}} + d\mathcal{X}. \quad (137)$$

By definition,

$$\begin{aligned} \dot{P} &= \frac{\partial}{\partial \dot{F}} \langle \langle W^* \rangle \rangle = \left\langle \left\langle \frac{\partial W^*}{\partial \dot{F}} \right\rangle \right\rangle = \left\langle \left\langle \left( \frac{\partial \dot{F}}{\partial \dot{F}} \right)^T \frac{\partial W^*}{\partial \dot{F}} \right\rangle \right\rangle \\ &= \left\langle \left\langle \left( I + \Gamma_h S \frac{\partial \mathcal{X}}{\partial \dot{F}} \right)^T \dot{P} \right\rangle \right\rangle = \langle \langle \dot{P} \rangle \rangle + \left( \frac{\partial \mathcal{X}}{\partial \dot{F}} \right)^T \langle \langle (\Gamma_h S)^T \dot{P} \rangle \rangle, \end{aligned} \quad (138)$$

where  $I$  denotes an identity matrix. Substituting the rate form of Eq. (133) into Eq. (138) gives

$$\dot{P} = \langle \langle \dot{P} \rangle \rangle \quad \text{or} \quad \bar{P} = \int_0^t \dot{P} dt = \int_0^t \langle \langle \dot{P} \rangle \rangle dt = \langle \langle P \rangle \rangle. \quad (139)$$

Next consider the outer loop.  $\bar{P}$  and  $\bar{F}$  can be partitioned as

$$\bar{P} = \begin{Bmatrix} \bar{P}_u \\ \bar{P}_k \end{Bmatrix} \quad \text{and} \quad \bar{F} = \begin{Bmatrix} \bar{F}_k \\ \bar{F}_u \end{Bmatrix}, \quad (140)$$

respectively. Let

$$\bar{P}^* = \begin{Bmatrix} \bar{P}_u \\ \bar{F}_u \end{Bmatrix} \quad \text{and} \quad \bar{F}^* = \begin{Bmatrix} \bar{F}_k \\ \bar{P}_k \end{Bmatrix}, \quad (141)$$

respectively. Set  $\bar{P}^*$  to be the variable, and choose

$$\Psi_{\text{out}}(\bar{P}^*) = \bar{F}^*(\bar{P}^*) - \bar{F}^* \quad (142)$$

as the function to be zeroed in the outer loop, where  $\bar{F}^*$  denotes the prescribed value of  $\bar{F}^*$  in the current load step. Requires

$$\Psi_{\text{out}}(\bar{P}_{\text{old}}^* + d\bar{P}^*) = \bar{F}^*(\bar{P}_{\text{old}}^*) + d\bar{F}^* - \bar{F}^* = 0. \quad (143)$$

Substituting Eq. (142) into Eq. (143) gives

$$d\bar{F}^* = -\Psi_{\text{out}}(\bar{P}_{\text{old}}^*). \quad (144)$$

The problem can then be solved by relating  $d\bar{P}^*$  to  $d\bar{F}^*$ . Combining Eqs. (92) and (139) gives

$$d\bar{P} = \langle \langle dP \rangle \rangle = \left\langle \left\langle \frac{\partial P}{\partial \dot{F}} \frac{\partial \dot{F}}{\partial \bar{F}} \right\rangle \right\rangle d\bar{F} = \langle \langle D \rangle \rangle d\bar{F} \equiv \bar{J} d\bar{F}, \quad (145)$$

where the third equality holds because  $\mathcal{X}$  is held fixed. Eq. (145) can be partitioned as

$$\begin{Bmatrix} d\bar{P}_u \\ d\bar{P}_k \end{Bmatrix} = \begin{bmatrix} \bar{J}_{uk} & \bar{J}_{uu} \\ \bar{J}_{kk} & \bar{J}_{ku} \end{bmatrix} \begin{Bmatrix} d\bar{F}_k \\ d\bar{F}_u \end{Bmatrix}. \quad (146)$$

Rearranging Eq. (146) gives

$$\begin{Bmatrix} d\bar{P}_u \\ d\bar{F}_u \end{Bmatrix} = \begin{bmatrix} \bar{J}_{uk} - \bar{J}_{uu}\bar{J}_{ku}^{-1}\bar{J}_{kk} & \bar{J}_{uu}\bar{J}_{ku}^{-1} \\ -\bar{J}_{ku}^{-1}\bar{J}_{kk} & \bar{J}_{ku}^{-1} \end{bmatrix} \begin{Bmatrix} d\bar{F}_k \\ d\bar{P}_k \end{Bmatrix} \quad (147)$$

or

$$d\bar{P}^* = \bar{J}^* d\bar{F}^*. \quad (148)$$

Premultiplying both sides of Eq. (144) by  $\bar{J}^*$  gives

$$d\bar{P}^* = -\bar{J}^* \Psi_{\text{out}}(\bar{P}_{\text{old}}^*). \quad (149)$$

The corrections can then be computed and added to the solution, i.e.,

$$\bar{P}_{\text{new}}^* = \bar{P}_{\text{old}}^* + d\bar{P}^*. \quad (150)$$

The whole process is iterated to convergence.

## IX. Numerical Examples

Zhang and Moore<sup>18</sup> performed a series of monotonic/cyclic uniaxial compression tests on high density polyethylene (HDPE), at different strain rates. These test data are appealing for model calibration and validation due to the following reason: the monotonic test data are suitable for model calibration, and the calibrated model can then be used to reproduce the cyclic test data. First, the constitutive model is calibrated via monotonic uniaxial compression tests on a polymer, and the calibrated model is validated by comparing its predictions with the remaining of the experimental data. Then, the micromechanics approach's capabilities are demonstrated through homogenizing a UDFRC with an HDPE matrix, subjected to uniaxial, biaxial, and shear loading, at different strain rates.

### A. HDPE

Choose the loading direction as the  $x_1$ -direction. Following Refs. [4, 18], assume that isotropic HDPE:

- has a Poisson's ratio ( $\nu_0$ ) of 0.39
- obeys the von Mises yield function along with an associated flow rule ( $\alpha = \beta = 0$  in Eqs. (158) and (160))
- exhibits the Voce hardening law, Eq. (161) (i.e., isotropic hardening but no kinematic hardening)

These assumptions are made due to a lack of sufficient experimental data. The effects of these assumptions will be discussed later this section. Figure 4 shows the experimental monotonic stress–strain curves of HDPE at a strain rate of  $10^{-4} \text{ s}^{-1}$ , and Figure 5 at a strain rate of  $10^{-3} \text{ s}^{-1}$ . Numerical experiments indicate that two branches in the generalized Maxwell model (i.e.,  $i = 0, 1$ ) are sufficient to characterize the viscoelastic behavior of HDPE. To reduce the complexity of calibration, assume that  $k_1 = g_1$ . The fitted viscoelastic parameters are then  $E_0$ ,  $K_1$ ,  $G_1$ , and  $k_1 = g_1$ . Thanks to viscous effects, viscoplasticity seldom affects the stress–strain relationships right after the onset of yielding. The initial yield stress,  $\sigma_y$ , then need not be exactly determined but can take an estimated value. Numerical experiments indicate that  $\sigma_y = 5 \text{ MPa}$  serves the purpose well.

In this work, the method of nonlinear least squares (NLLSQ), which contains Monte Carlo experiments and Powell's methods, is used (see Appendix D for more details). The calibration process consists of the following major steps:

1. Calibrate the viscoelastic parameters (see Table 1(a)) from the first 5 to 6 data points in Figures 4 and 5.
2. Hold the viscoelastic parameters fixed, and calibrate the viscoplastic parameters (see Table 1(a)) from the remaining data points in the loading segments in Figures 4 and 5.

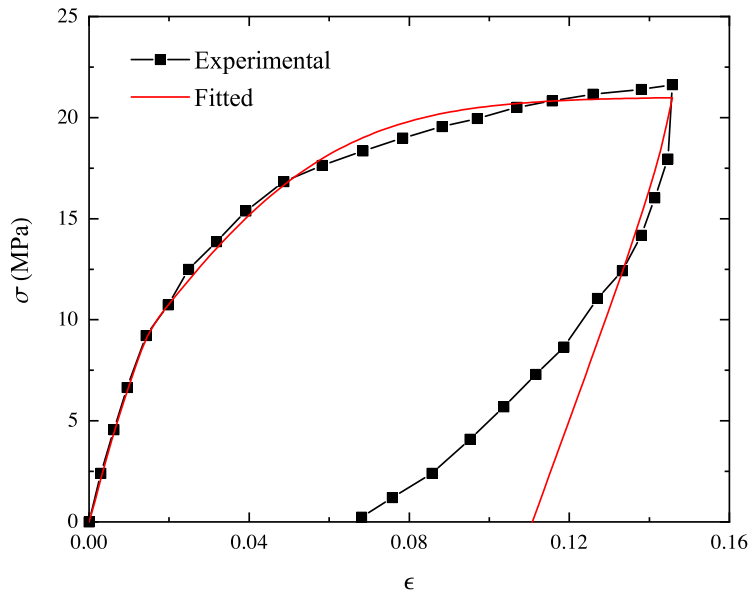


Figure 4. Experimental and fitted monotonic stress–strain curves of HDPE at a strain rate of  $10^{-4} \text{ s}^{-1}$ .

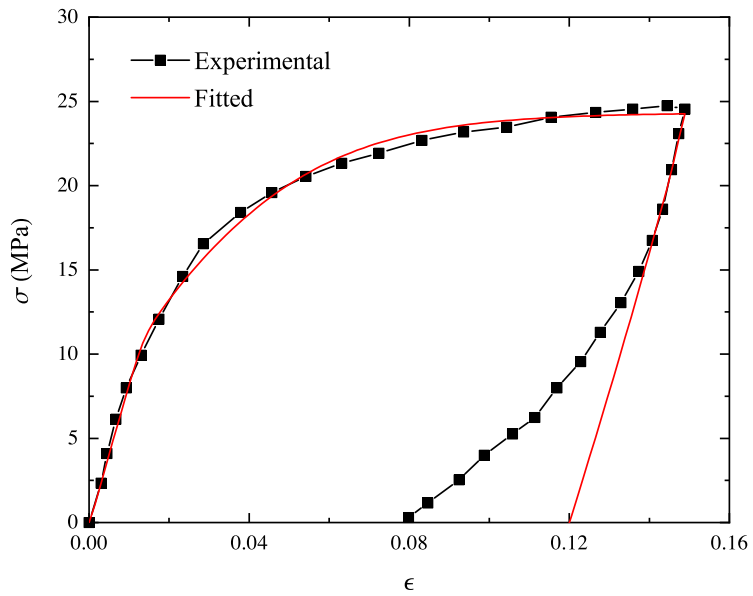


Figure 5. Experimental and fitted monotonic stress–strain curves of HDPE at a strain rate of  $10^{-3} \text{ s}^{-1}$ .

3. Fine-tune all material parameters to make the predicted curves have the best fit to the experimental ones.

This “staggered” method can be used time by time throughout a calibration process. Especially, Step 1 is accomplished as follows:

1. Set  $K_1 = G_1 = 0$ , and calibrate  $E_0$  from the data points.
2. Hold  $E_0$  fixed, and calibrate  $K_1$  and  $G_1$  from the data points.
3. Fine-tune  $E_0$ ,  $K_1$ , and  $G_1$  to make the predicted curves have the best fit to the data points.

Table 1 lists the fitted parameters of HDPE, and Figures 4 and 5 compare the fitted curves with the experimental ones. Each curve in Figures 4 and 5 can be divided into a loading segment and an unloading segment. As can be seen:

- Each fitted loading segment agree with its corresponding experimental one very well.
- Each fitted unloading segment does not agree with its corresponding experimental one.

Recall that only the loading segments were considered during calibration. The first point indicates that the calibrated constitutive model can reproduce the test data. In contrast, the reason for the second point is that the unloading segments were not considered during calibration. On the one hand, this can be further improved by devoting more time and efforts to calibration. On the other hand, the following is worth noting:

- Each fitted unloading segment exhibits an approximately linear trend.
- Each experimental unloading segment exhibits a nonlinear trend at an early stage of unloading.

These experimental data indicate that HDPE may exhibit not only isotropic hardening but also kinematic hardening. Given experimental evidence indicating that polymers often exhibit kinematic hardening, it is necessary to incorporate kinematic hardening into the constitutive model in further work.

**Table 1. Material parameters of HDPE.**

(a) Viscoelastic parameters.				
$E_0$ (MPa)	$\nu_0$	$K_1$ (MPa)	$G_1$ (MPa)	$k_1 = g_1$ (s)
543.198	0.39	488.225	115.91	55.5891

(b) Viscoplastic parameters.				
$\sigma_y$ (MPa)	$Q$ (MPa)	$b$	$\gamma$ ( $s^{-1}$ )	$n$
5	5.50879	53.2535	$1.00845 \times 10^{-4}$	8.27066

The calibrated constitutive model is then used to predict the responses of HDPE experiencing different loading paths. Figure 6 compares the predicted cyclic stress–strain curve at a strain rate of  $10^{-4} s^{-1}$ , with the experimental one. Each curve can be divided into a series of loading, unloading, and reloading segments. The predicted initial loading segment agrees well with the experimental one. As HDPE is further deformed, the subsequent predicted unloading and reloading segments increasingly deviate from their respective experimental ones. This may again be because HDPE exhibits not only isotropic hardening but also kinematic hardening, causing the experimental unloading segments to be highly nonlinear.

Figure 7 compares the predicted varying-strain-rate stress–strain curves with the experimental one. Here the loading path consists of the following steps:

1. initial loading—HDPE is loaded up to an elongation of 1.65%, at a strain rate of  $10^{-4} s^{-1}$
2. relaxation—HDPE is held fixed at an elongation of 1.65%, for 450 s
3. reloading—HDPE is loaded up to an elongation of 3.5%, at a strain rate of  $10^{-2} s^{-1}$

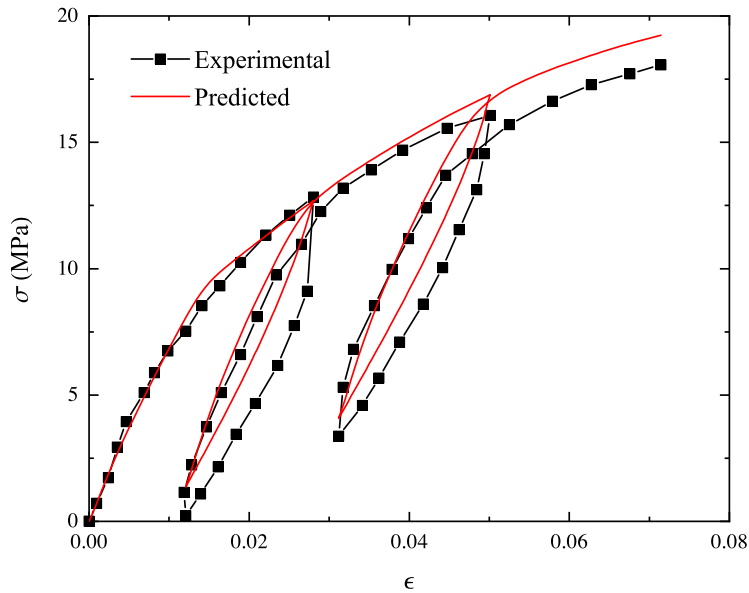


Figure 6. Experimental and predicted cyclic stress–strain curves of HDPE at a strain rate of  $10^{-4} \text{ s}^{-1}$ .

As can be seen:

1. The predicted initial loading segment agrees well with the experimental one.
2. The predicted relaxation segment is shorter than the experimental one.
3. The predicted reloading segment noticeably deviate from the experimental one.

The second point indicates that the fitted viscoelastic parameters cannot well describe the responses of HDPE during relaxation. The deviation during relaxation further causes the subsequent deviation during reloading. In conclusion, Figures 6 and 7 indicate that the fitted parameters can well describe the responses of HDPE during loading but not those during unloading or relaxation. The material parameters can be better calibrated through the following:

- Incorporate kinematic hardening into the constitutive model.
- Consider more strain rates during calibration, to better calibrate the viscoelastic parameters.
- Conduct cyclic tests rather than monotonic tests to better calibrate the viscoplastic parameters.

Especially, cyclic tests are preferable to monotonic tests because each of its unloading segment helps one:

- determine the current residual/viscoplastic strain
- isolate the effects of viscoelasticity and viscoplasticity
- calibrate viscoelastic and viscoplastic parameters separately and therefore more accurately

## B. UDFRC

Next consider a UDFRC consisting of an HDPE matrix (with its material parameters calibrated above) and numerous cylindrical, elastic fibers arranged in a square array. For demonstration purposes, the volume fraction of fibers is set to be 10%. This is because:

- There is a lack of experimental data for composite-level calibration or validation.
- Only HDPE contributes to the composite’s material nonlinearity and rate dependence.

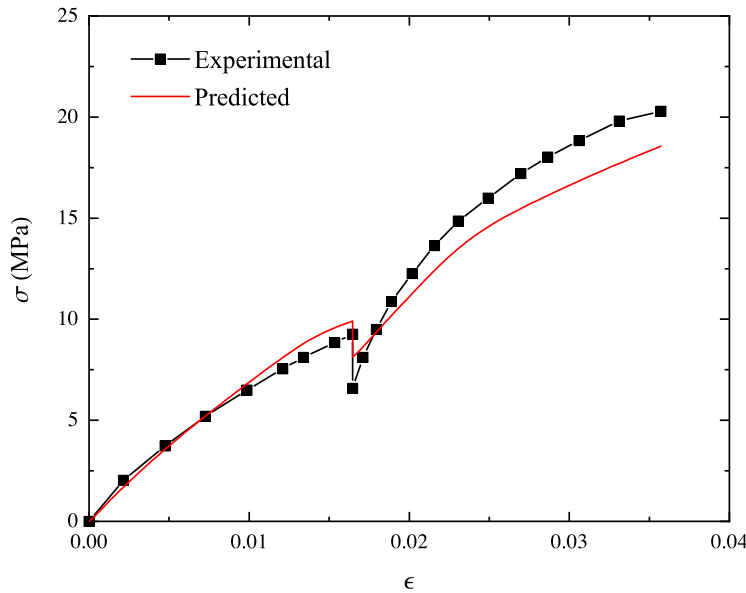


**Figure 7. Experimental and predicted varying-strain-rate stress–strain curves of HDPE.**

Let the fibers have a Young’s modulus of 76 GPa and a Poisson’s ratio of 0.22. Let the SG of this composite consist of a square matrix and a circular fiber located at its center. Choose the center of the SG as the origin of the local coordinates,  $y_i$ , and the fiber direction and the length and width directions of the SG as the  $y_1$ -, the  $y_2$ -, and the  $y_3$ -directions, respectively.

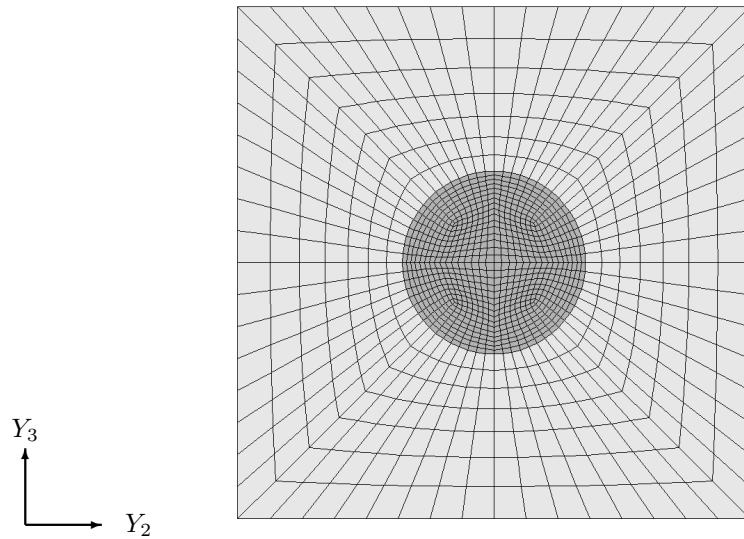
Figure 8(a) depicts the SG used in the micromechanics approach. The 2D SG is meshed with 4-node quadrilateral elements with 3 degrees of freedom (DOFs) at each node, and the meshed SG consists of 1216 elements. This FE model is found to be capable of producing converged results. In contrast, to simulate longitudinal shear deformation using FE analysis (FEA), one has to at least use a 3D SG as shown in Figure 8(b). The 3D SG is meshed with 8-node hexahedral elements, and the meshed SG consists of 2432 elements. Both FE models are found to be capable of producing converged results. Clearly, a 2D SG can have much less DOFs than a 3D SG and therefore reduce the computational effort.

Figure 9 shows the stress–strain hysteresis loops of the composite subjected to uniaxial loading in the  $y_1$ - and the  $y_2$ -directions, respectively. Hereafter let each loading path consist of the following steps:

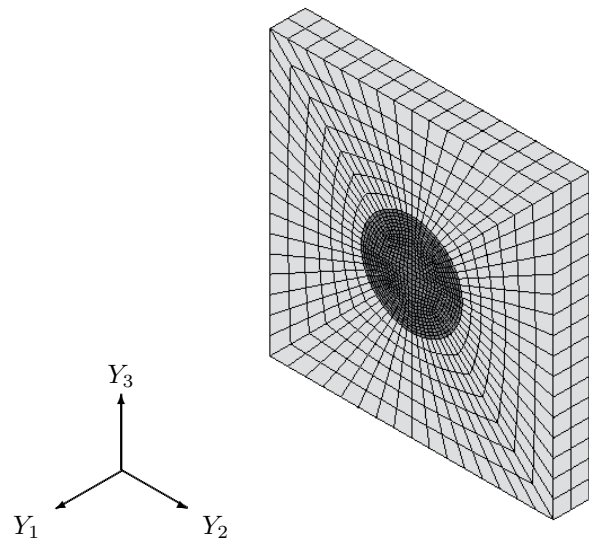
1. initial loading—the major strain(s) is increased from 0 to 0.1
2. initial unloading—the major strain(s) is decreased from 0.1 to 0
3. reverse loading—the major strain(s) is decreased from 0.0 to  $-0.1$
4. reverse unloading—the major strain(s) is increased from  $-0.1$  to 0

It can be seen that the composite exhibits an approximately linear stress–strain relationship when loaded in the  $y_1$ -direction and a highly nonlinear one when loaded in the  $y_2$ -direction. This can be understood by investigating the stress distribution in the SG. In Figure 9(a), the fiber sustains most of the external load, and accordingly, the composite behaves like a linearly elastic fiber. In Figure 9(b), the matrix also sustains the external load, and the stress distribution in the matrix remains highly nonuniform. All these cause the matrix to yield successively at different locations. In addition, in Figure 9(b), the composite becomes stiffer as the major strain rate increases. This agrees with the theory of viscoplasticity. In contrast, in Figure 9(a), the composite seldom exhibits any rate dependence. This is again because here the rate-independent fiber sustains most of the external load.

Figure 10 shows the stress–strain hysteresis loops of the composite subjected to equal biaxial loading in the  $y_2y_3$  plane. It can be seen that the composite exhibits an approximately bilinear stress–strain relationship during initial loading and a nonlinear stress–strain relationship at the beginning of unloading/reverse loading. This can be understood by investigating the matrix deformation. During initial loading, the matrix undergoes

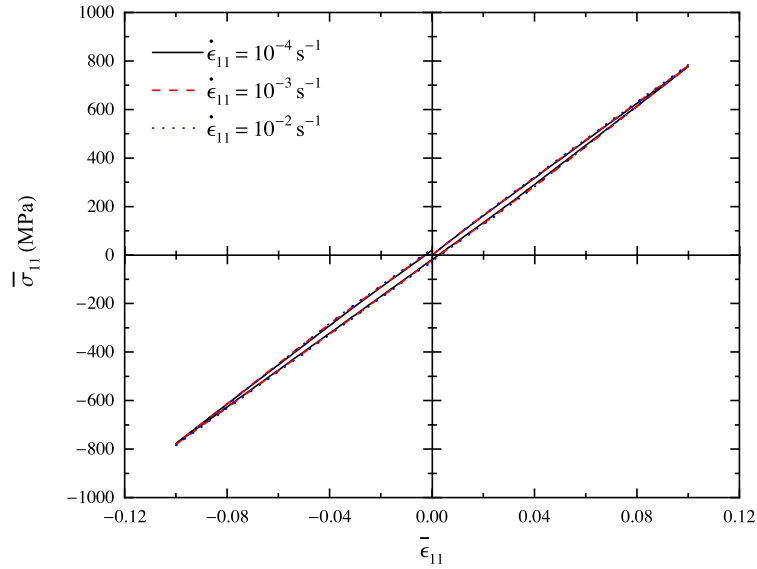


(a) Micromechanics approach.

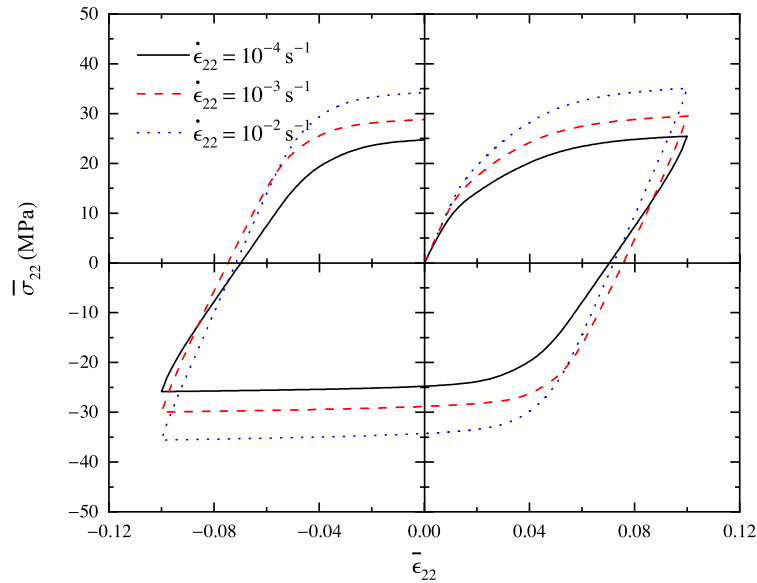


(b) FEA.

**Figure 8. Meshed SGs of a UDRFC.**



(a)  $y_1$ -direction.



(b)  $y_2$ -direction.

Figure 9. Stress–strain hysteresis loops of a UDRFC subjected to uniaxial loading.

first entirely viscoelastic deformation and then viscoelastic-viscoplastic deformation. At the beginning of unloading/reverse loading, the matrix still undergoes viscoelastic-viscoplastic deformation because the over stress (i.e.,  $f$  in Eq. (55)) has not dropped below zero. All these leads to different stress–strain relationships. In addition, the composite also exhibits prominent rate dependence. This is because here the matrix also sustains the external load.

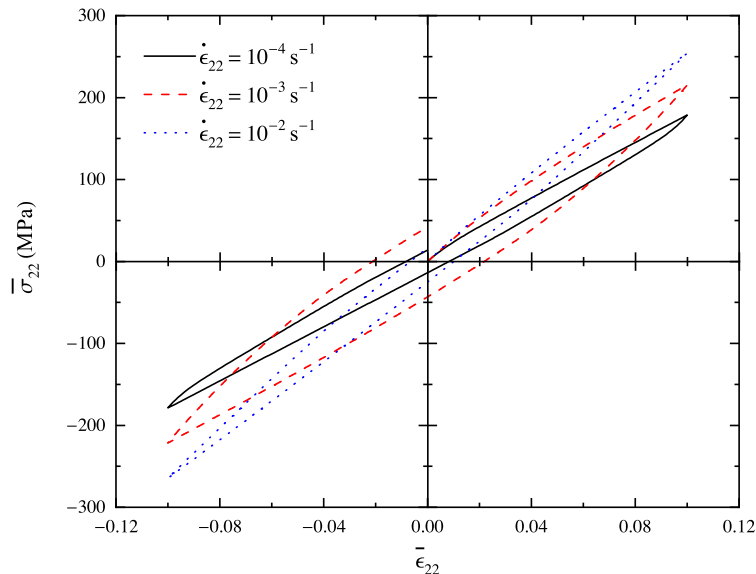


**Figure 10. Stress–strain hysteresis loops of a UDRFC subjected to equal biaxial loading in the  $y_2y_3$  plane.**

Figure 11(a) shows the stress–strain hysteresis loops of the composite subjected to transverse shear loading, and Figure 11(b) depicts an SG undergoing exaggerated deformation. It can be seen that the stress–strain relationships here are similar to those in Figure 9(b). Therefore, the discussion for Figure 9(b) holds here. However, the stress levels here are much lower than those in Figure 9(b). This is because the matrix more easily yields under pure shear than under other loading conditions, such as uniaxial loading.

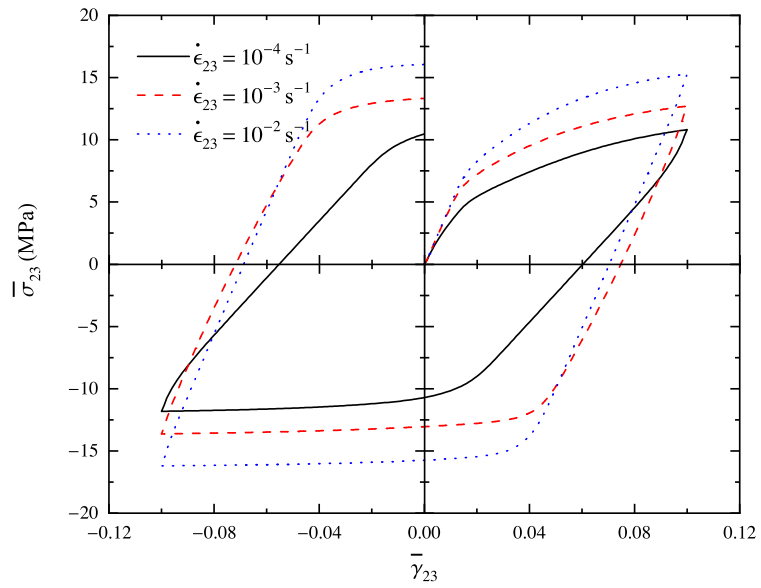
Figure 12(a) shows the stress–strain hysteresis loops of the composite subjected to longitudinal shear loading, and Figure 12(b) depicts an SG undergoing exaggerated deformation. It can be seen that the stress–strain relationships here are similar to those in Figures 9(b) and 11(a). Therefore, the discussion for Figure 9(b) and 11(a) holds here. As mentioned above, to simulate longitudinal shear loading using FEA, one has to at least use a 3D SG. This can be better understood by noting that, in Figure 12(b), the local displacements fluctuate in the  $y_1$ -direction due to the existence of the fiber. This indicates that, compared with FEA, the micromechanics approach can often homogenize a composite in a simpler and more efficient way.

## X. Conclusions

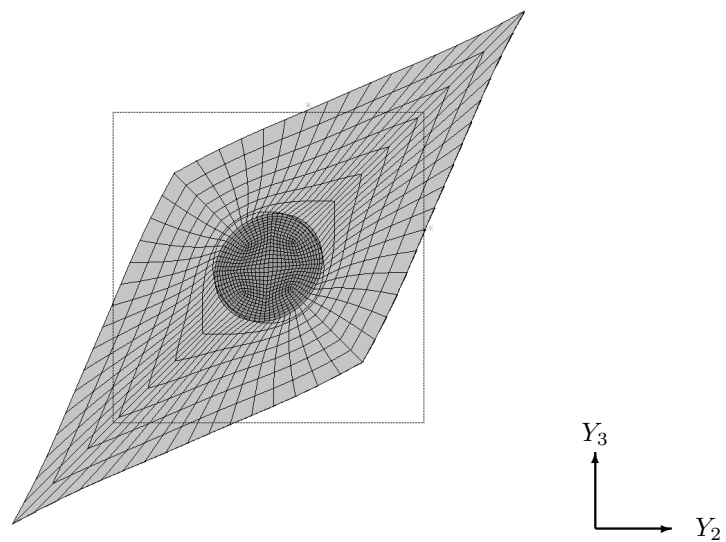
In this paper, a constitutive model for finitely deformed viscoelastic-viscoplastic materials is developed, and a micromechanics approach to homogenizing composites consisting of such materials is developed subsequently. The development of the constitutive model involves establishing a thermodynamic framework based on finite strain theory, developing a viscoelasticity and a viscoplasticity model based on the thermodynamic framework, developing a radial return algorithm based on a classic framework, and deriving a closed-form incremental constitutive relation in the spatial configuration. The development of the micromechanics approach involves pulling-back the above constitutive relation to the material configuration, formulating a variational statement with the resulting constitutive relation, discretizing variational statement in a finite-dimensional space, and solving the discretized variational statement using an Euler–Newton predictor–corrector method.

The following findings can be obtained from the results:

- The calibrated constitutive model is shown capable of accurately predicting the responses of HDPE

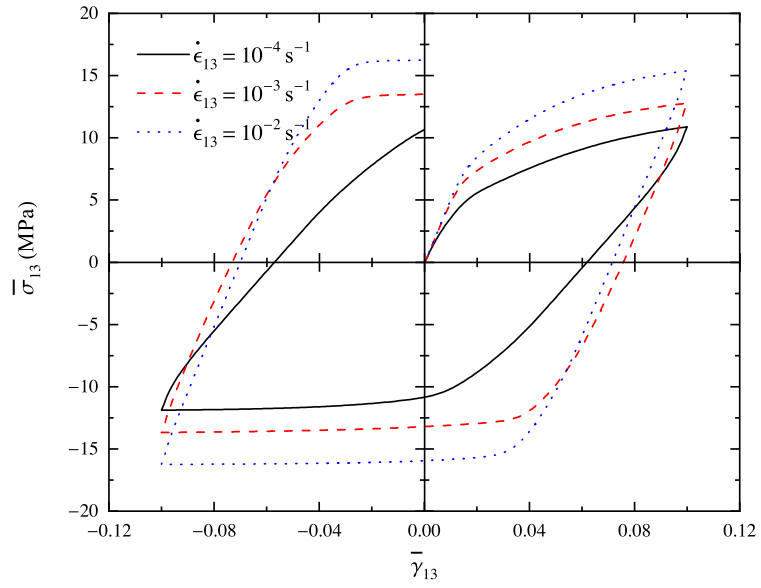


(a) Stress-strain hysteresis loops.

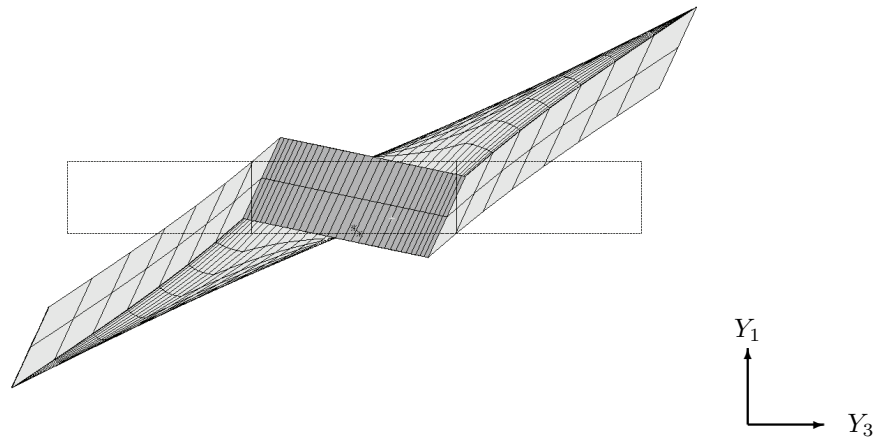


(b) Deformed shape and undeformed edge.

**Figure 11. UDRFC subjected to transverse shear loading.**



(a) Stress-strain hysteresis loops.



(b) Deformed shape and undeformed edge.

**Figure 12.** UDRFC subjected to longitudinal shear loading.

during loading but not those during unloading or relaxation.

- The closed-form incremental constitutive relation is found to facilitate model calibration and implementation.
- The micromechanics approach is demonstrated to be capable of handling rate dependence and complex loading paths.

The constitutive model can be conveniently implemented in an FE code, to perform structural analysis. The material parameters can be better calibrated through the following:

- Incorporate kinematic hardening into the constitutive model.
- Consider more strain rates during calibration, to better calibrate the viscoelastic parameters.
- Conduct cyclic tests rather than monotonic tests to better calibrate the viscoplastic parameters.

The micromechanics approach can be embedded in a multiscale modeling framework, to perform multiscale modeling. The present framework can be further improved by implementing more sophisticated viscoelasticity and viscoplasticity models in future work.

## Acknowledgments

The views and conclusions contained herein are those of the authors and should not be interpreted as necessarily representing the official policies or endorsement, either expressed or implied, of the sponsor.

### A. 1D Viscoelasticity Model

In this appendix:

- Omit the superscript/subscript “*ve*” as the deformation is entirely viscoelastic.
- Abandon the Einstein summation convention unless otherwise specified—most sums are indicated by summation signs.

Figure 13 depicts a 1D generalized Maxwell model, where:

- $E_i$  ( $i = 0, 1, \dots, N$ )—Young’s modulus of the  $i^{\text{th}}$  spring
- $\eta_i$  ( $i = 1, 2, \dots, N$ )—viscosity of the  $i^{\text{th}}$  dashpot
- $\tau$ —stress acting on the network
- $\epsilon$ —strain in the network (and therefore in each branch)
- $\tau_0$ —stress acting on the zeroth spring
- $q_i$  ( $i = 1, 2, \dots, N$ )—stress acting on the  $i^{\text{th}}$  branch
- $\gamma_i$  ( $i = 1, 2, \dots, N$ )—strain in the  $i^{\text{th}}$  dashpot

The following can be obtained from Figure 13:

$$\tau = \tau_0 + \sum_{i=1}^N q_i, \quad (151)$$

$$\tau_0 = E_0 \epsilon, \quad (152)$$

$$q_i = E_i (\epsilon - \gamma_i) = \eta_i \dot{\gamma}_i. \quad (153)$$

The following can be obtained from Eq. (153):

$$\dot{q}_i + \frac{q_i}{s_i} = E_i \dot{\epsilon}, \quad (154)$$

where  $s_i = \eta_i/E_i$  is the characteristic relaxation time of the  $i^{\text{th}}$  branch.  $\hat{\Psi}$  can then be expressed as the sum of its  $N + 1$  parts each of which represents a branch, i.e.,

$$\hat{\Psi}(\epsilon, \gamma_1, \dots, \gamma_N) = \hat{\Psi}_0(\epsilon) + \sum_{i=1}^N \hat{\Psi}_i(\epsilon, \gamma_i), \quad (155)$$

where

$$\hat{\Psi}_0(\epsilon) = \frac{1}{2}E_0\epsilon^2 \quad \text{and} \quad \hat{\Psi}_i(\epsilon, \gamma_i) = \frac{1}{2}E_i(\epsilon - \gamma_i)^2. \quad (156)$$

The following can be verified:

$$\tau = \frac{\partial \hat{\Psi}}{\partial \epsilon} = \frac{d\hat{\Psi}_0}{d\epsilon} + \sum_{i=1}^N \frac{\partial \hat{\Psi}_i}{\partial \epsilon} \quad \text{and} \quad q_i = -\frac{\partial \hat{\Psi}}{\partial \gamma_i} = -\frac{\partial \hat{\Psi}_i}{\partial \gamma_i}. \quad (157)$$

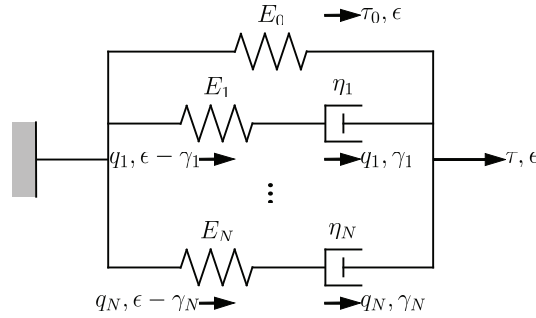


Figure 13. 1D generalized Maxwell model (adapted from Ref. [19]).

## B. Drucker–Prager Yield Function

Let yield function  $f$  be the Drucker–Prager yield function, i.e.,

$$f(\boldsymbol{\tau}, R) = \frac{1}{1 - \alpha} (\|\boldsymbol{\tau}'\| + 3\alpha\tau_m) - \tau_c - R, \quad (158)$$

where

$$\|\boldsymbol{\tau}'\| = \sqrt{\frac{3}{2}\boldsymbol{\tau}' : \boldsymbol{\tau}'}, \quad \alpha = \frac{\tau_c - \tau_t}{\tau_c + \tau_t}, \quad (159)$$

and  $\tau_c$  and  $\tau_t$  denote the initial yield stress in uniaxial compression and that in uniaxial tension, respectively. Without loss of generality, set

$$F(\boldsymbol{\tau}, R) = C(\|\boldsymbol{\tau}'\| + 3\beta\tau_m) - \tau_c - R, \quad (160)$$

where  $\beta$  is a parameter describing dilatancy, and  $C$  is a constant to be determined. Eq. suggests that  $R(r)$  is measured via the uniaxial compression test. Set  $R(r)$  to be the Voce hardening law,<sup>20</sup> i.e.,

$$R = Q[1 - \exp(-br)], \quad (161)$$

where  $Q$  and  $n$  are two isotropic hardening parameters.

$\mathbf{n}$ ,  $C$ ,  $\mathbf{N}$ , and  $\partial \mathbf{N} / \partial \boldsymbol{\tau}$  are to be determined. Differentiating both sides of the equation with respect to  $\boldsymbol{\tau}$  gives

$$\mathbf{n} = \frac{1}{1 - \alpha} \left( \frac{\partial \|\boldsymbol{\tau}'\|}{\partial \boldsymbol{\tau}} + 3\alpha \frac{\partial \tau_m}{\partial \boldsymbol{\tau}} \right). \quad (162)$$

The partial derivatives in Eq. (162) can be expressed as

$$\frac{\partial \|\boldsymbol{\tau}'\|}{\partial \boldsymbol{\tau}} = \frac{1}{2\|\boldsymbol{\tau}'\|} \frac{\partial \|\boldsymbol{\tau}'\|^2}{\partial \boldsymbol{\tau}} = \frac{1}{2\|\boldsymbol{\tau}'\|} \left( \frac{3}{2} \frac{\partial \boldsymbol{\tau}'}{\partial \boldsymbol{\tau}} : \boldsymbol{\tau}' \right) = \frac{3\boldsymbol{\mathcal{I}}' : \boldsymbol{\tau}'}{2\|\boldsymbol{\tau}'\|} = \frac{3\boldsymbol{\tau}'}{2\|\boldsymbol{\tau}'\|}, \quad (163)$$

$$\frac{\partial \tau_m}{\partial \boldsymbol{\tau}} = \frac{\partial}{\partial \boldsymbol{\tau}} \left( \frac{\boldsymbol{\tau} : \mathbf{I}}{3} \right) = \frac{\mathbf{I}}{3}. \quad (163')$$

Substituting Eq. (163) into Eq. (162) gives

$$\mathbf{n} = \frac{1}{1-\alpha} \left( \frac{3\boldsymbol{\tau}'}{2\|\boldsymbol{\tau}'\|} + \alpha\mathbf{I} \right). \quad (164)$$

Similarly,  $\mathbf{N}$  can be expressed as

$$\mathbf{N} = C \left( \frac{3\boldsymbol{\tau}'}{2\|\boldsymbol{\tau}'\|} + \beta\mathbf{I} \right), \quad (165)$$

where  $C$  is still to be determined. Suppose that the material is subjected to uniaxial tension/compression in the  $x_1$ -direction, for which  $\boldsymbol{\tau}$  takes the form of

$$\boldsymbol{\tau} = \tau_{11}\mathbf{e}_1 \otimes \mathbf{e}_1. \quad (166)$$

Substituting Eqs. (162) and (166) into the first equation of Eq. (26) gives

$$\dot{\epsilon}_{11}^{vp} = \begin{cases} \dot{v}C(1+\beta) & \tau_{11} > 0, \\ -\dot{v}C(1-\beta) & \tau_{11} < 0. \end{cases} \quad (167)$$

Set  $|\epsilon_{11}^{vp}| = r$  so that the isotropic hardening parameters can be conveniently calibrated via cyclic uniaxial tension/compression tests. Substituting  $|\dot{\epsilon}_{11}^{vp}| = \dot{r} = \dot{v}$  into Eq. (167) gives

$$C = \begin{cases} \frac{1}{1+\beta} & \tau_{11} > 0, \\ \frac{1}{1-\beta} & \tau_{11} < 0, \end{cases} \quad (168)$$

which indicates that the value of  $C$  depends on whether one calibrates the model via the tension or the compression test. Eq. (158) suggests that  $C = \frac{1}{1-\beta}$  here. Eq. (165) can then be rewritten as

$$\mathbf{N} = \frac{1}{1-\beta} \left( \frac{3\boldsymbol{\tau}'}{2\|\boldsymbol{\tau}'\|} + \beta\mathbf{I} \right). \quad (169)$$

Differentiating  $\boldsymbol{\tau}'/\|\boldsymbol{\tau}'\|$  with respect to  $\boldsymbol{\tau}$  gives

$$\begin{aligned} \frac{\partial}{\partial \boldsymbol{\tau}} \left( \frac{\boldsymbol{\tau}'}{\|\boldsymbol{\tau}'\|} \right) &= \boldsymbol{\tau}' \otimes \frac{\partial}{\partial \boldsymbol{\tau}} \left( \frac{1}{\|\boldsymbol{\tau}'\|} \right) + \frac{1}{\|\boldsymbol{\tau}'\|} \frac{\partial \boldsymbol{\tau}'}{\partial \boldsymbol{\tau}} \\ &= \boldsymbol{\tau}' \otimes \left( -\frac{1}{\|\boldsymbol{\tau}'\|^2} \frac{\partial \|\boldsymbol{\tau}'\|}{\partial \boldsymbol{\tau}} \right) + \boldsymbol{\mathcal{I}}' = \frac{1}{\|\boldsymbol{\tau}'\|} \left( \boldsymbol{\mathcal{I}}' - \frac{3\boldsymbol{\tau}' \otimes \boldsymbol{\tau}'}{2\|\boldsymbol{\tau}'\|^2} \right). \end{aligned} \quad (170)$$

$\partial \mathbf{N} / \partial \boldsymbol{\tau}$  can then be expressed as

$$\frac{\partial \mathbf{N}}{\partial \boldsymbol{\tau}} = \frac{3}{2(1-\beta)\|\boldsymbol{\tau}'\|} \left( \boldsymbol{\mathcal{I}}' - \frac{3\boldsymbol{\tau}' \otimes \boldsymbol{\tau}'}{2\|\boldsymbol{\tau}'\|^2} \right). \quad (171)$$

### C. Principal Stretches and Unit Vectors

In this appendix, some derivation regarding the principal stretches and their unit vectors will be presented. For brevity, assume that there are three different  $\lambda_A$ 's unless otherwise specified. First consider the derivation of Eq. (115). Similarly to Eq. (32),  $\mathbf{C}$  can be decomposed as

$$\mathbf{C} = \sum_{A=1}^3 \lambda_A^2 \mathbf{P}_A \otimes \mathbf{P}_A, \quad (172)$$

where  $\mathbf{P}_A$  denotes the  $A^{\text{th}}$  principal unit vector of  $\mathbf{C}$ .  $\mathbf{P}_A$  can be related to  $\mathbf{p}_A$  by

$$\mathbf{F} \cdot \mathbf{P}_A = \lambda_A \mathbf{p}_A. \quad (173)$$

By definition,

$$\mathbf{C} \cdot \mathbf{P}_A = \lambda_A^2 \mathbf{P}_A \quad \text{and} \quad \mathbf{b} \cdot \mathbf{p}_A = \lambda_A^2 \mathbf{p}_A. \quad (174)$$

Totally differentiating both sides of the first equation of Eq. (174) gives

$$d\mathbf{C} \cdot \mathbf{P}_A + \mathbf{C} \cdot d\mathbf{P}_A = 2\lambda_A d\lambda_A \mathbf{P}_A + \lambda_A^2 d\mathbf{P}_A. \quad (175)$$

Premultiplying both sides of Eq. (175) by  $\mathbf{P}_A$  gives

$$\mathbf{P}_A \cdot d\mathbf{C} \cdot \mathbf{P}_A + \mathbf{P}_A \cdot \mathbf{C} \cdot d\mathbf{P}_A = 2\lambda_A d\lambda_A \mathbf{P}_A \cdot \mathbf{P}_A + \lambda_A^2 \mathbf{P}_A \cdot d\mathbf{P}_A. \quad (176)$$

Note the following:

- By definition,  $\mathbf{P}_A \cdot \mathbf{P}_A = 1$ .
- Totally differentiating both sides of  $\mathbf{P}_A \cdot \mathbf{P}_A = 1$  gives  $\mathbf{P}_A \cdot d\mathbf{P}_A = 0$ .
- Eq. (174) suggests that  $\mathbf{P}_A \cdot \mathbf{C} \cdot d\mathbf{P}_A = \lambda_A^2 \mathbf{P}_A \cdot d\mathbf{P}_A$ .

Eq. (176) then becomes

$$2\lambda_A d\lambda_A = \mathbf{P}_A \cdot d\mathbf{C} \cdot \mathbf{P}_A = d\mathbf{C} : (\mathbf{P}_A \otimes \mathbf{P}_A). \quad (177)$$

Totally differentiating both sides of Eq. (33) gives  $d\epsilon_A = d\lambda_A/\lambda_A$ . Eq. (177) can then be rewritten as

$$2\lambda_A^2 d\epsilon_A = d\mathbf{C} : (\mathbf{P}_A \otimes \mathbf{P}_A). \quad (178)$$

Noting that  $d\epsilon_A$  and  $d\mathbf{C}$  can be arbitrarily chosen gives

$$2 \frac{\partial \epsilon_A}{\partial \mathbf{C}} = \lambda_A^{-2} \mathbf{P}_A \otimes \mathbf{P}_A. \quad (179)$$

Premultiplying both sides of Eq. (179) by  $\mathbf{F}$  and postmultiplying both sides of the equation by  $\mathbf{F}^T$  (see also Eq. (173)) give

$$2\mathbf{F} \cdot \frac{\partial \epsilon_A}{\partial \mathbf{C}} \cdot \mathbf{F}^T = \mathbf{p}_A \otimes \mathbf{p}_A. \quad (180)$$

Next consider the explicit expression for  $\mathcal{R}_A$ . It is beneficial to first derive the explicit expression for  $\mathbf{q}_A$ . By definition,  $\lambda_A^2$ 's are the roots of characteristic polynomial

$$-\lambda^6 + I_1 \lambda^4 - I_2 \lambda^2 + I_3 = 0, \quad (181)$$

where

$$I_1 = \text{tr} \mathbf{C}, \quad I_2 = \frac{1}{2} [\text{tr}^2 \mathbf{C} - \text{tr}(\mathbf{C}^2)], \quad I_3 = \det \mathbf{C} = J^2 \quad (182)$$

are the first, second, and third invariants of  $\mathbf{C}$  (or  $\mathbf{b}$ ), respectively. The roots of the characteristic polynomial can be computed using the well-known closed-form solution of a cubic equation. If Eq. (181) has three different roots, the first equation of Eq. (32) can be rewritten as

$$\mathbf{b} - \lambda_A^2 \mathbf{I} = \sum_{B=1; B \neq A}^3 (\lambda_B^2 - \lambda_A^2) \mathbf{p}_B \otimes \mathbf{p}_B. \quad (183)$$

Noting that  $\mathbf{p}_A \cdot \mathbf{p}_B = \delta_{AB}$ , one can obtain the following from Eq. (183):

$$\mathbf{p}_A \otimes \mathbf{p}_A = \frac{\mathbf{b} - \lambda_B^2 \mathbf{I}}{\lambda_B^2 - \lambda_A^2} \cdot \frac{\mathbf{b} - \lambda_C^2 \mathbf{I}}{\lambda_C^2 - \lambda_A^2}, \quad (184)$$

where

$$A = 1, 2, 3, \quad B = 1 + \text{mod}(3, A), \quad C = 1 + \text{mod}(3, B). \quad (185)$$

Eq. (85) can be rewritten as

$$(\mathcal{R}_A)_{ijkl} = F_{im} F_{jn} F_{kp} F_{lq} \frac{\partial}{\partial C_{pq}} [F_{mr}^{-1} (p_A)_r (p_A)_s F_{sn}^{-T}]. \quad (186)$$

The explicit expression for  $\mathcal{R}_A$  can be obtained as follows:

1. Pull-back  $\mathbf{F}^{-1} \cdot (\mathbf{p}_A \otimes \mathbf{p}_A) \cdot \mathbf{F}^{-T}$  to the material configuration (i.e., express it in terms of  $\lambda_A$  and  $\mathbf{P}_A$ , with Eq. (173)).
2. Derive the explicit expression for  $\frac{\partial}{\partial \mathbf{C}} \left[ \mathbf{F}^{-1} \cdot (\mathbf{p}_A \otimes \mathbf{p}_A) \cdot \mathbf{F}^{-T} \right]$  in the material configuration.
3. Push-forward this explicit expression to the spatial configuration.

The explicit expression for  $\mathcal{R}_A$  reads

$$\begin{aligned} \mathcal{R}_A = \frac{1}{d_A} \left\{ \mathcal{I}^b - \mathbf{b} \otimes \mathbf{b} - I_3 \lambda_A^{-2} [\mathcal{I} - (\mathbf{I} - \mathbf{q}_A) \otimes (\mathbf{I} - \mathbf{q}_A)] \right\} \\ + \frac{\lambda_A^2}{d_A} [(\mathbf{b} \otimes \mathbf{q}_A + \mathbf{q}_A \otimes \mathbf{b}) + (I_1 - 4\lambda_A^2) \mathbf{q}_A \otimes \mathbf{q}_A], \end{aligned} \quad (187)$$

where

$$d_A = (\lambda_A^2 - \lambda_B^2) (\lambda_A^2 - \lambda_C^2) \quad (188)$$

with  $A$ ,  $B$ , and  $C$  given by Eq. (185), and

$$\mathcal{I}_{ijkl}^b = \frac{1}{2} (b_{ik} b_{jl} + b_{il} b_{jk}). \quad (189)$$

The derivation of Eq. (187) is omitted here due to its complexity. Interested readers can refer to Ref. [21] for more details. If two or three out of three  $\lambda_A$ 's are identical, it is possible to obtain results similar to Eqs. (180), (184), and (187). However, it is computationally favorable to convert this situation degenerates into the case of three distinct  $\lambda_A$ 's by superposing perturbations upon identical  $\lambda_A$ 's.

## D. Method of Nonlinear Least Squares

In this appendix, the method of NLLSQ, along with Monte Carlo experiments and Powell's methods, will be briefly introduced. Unless otherwise specified, let the "local" variables defined in this appendix override the "global" variables defined in Sections II–IX, having the same names.

Suppose that  $N$  data points  $(x_i, y_i)$ 's are to be fitted to a nonlinear model depending on  $M$  adjustable parameters  $a_j$ 's ( $N \geq M$ ). Let

$$\mathbf{a} = \left[ a_1 \quad \cdots \quad a_M \right]^T, \quad (190)$$

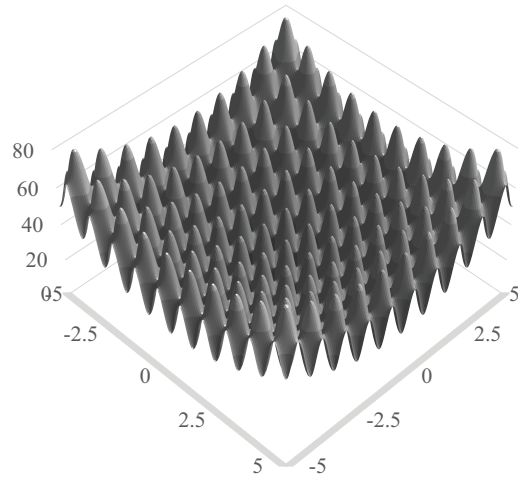
and let the nonlinear model take the general form of  $y = f(x; \mathbf{a})$ . Further suppose that each  $(x_i, y_i)$  has its respective, known standard deviation  $\sigma_i$ , and introduce the so-called chi-square merit function,

$$\chi^2 \equiv \sum_{i=1}^N \left( \frac{y_i - f(x_i; \mathbf{a})}{\sigma_i} \right)^2, \quad (191)$$

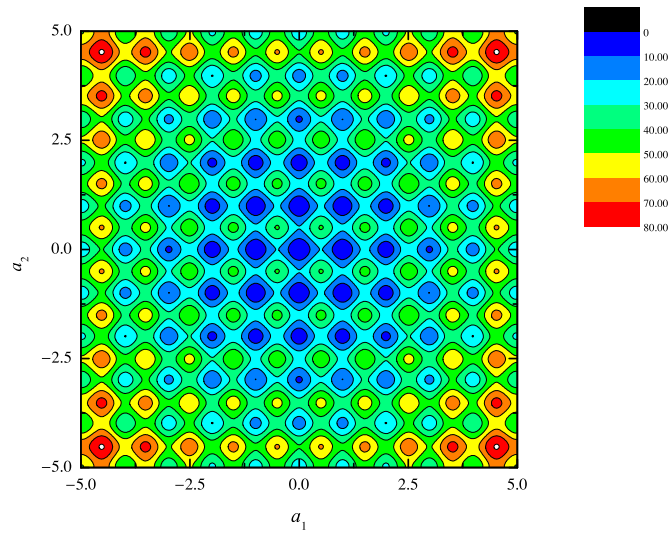
which is the sum of  $N$  squares of normalized, distributed residuals. The method of NLLSQ involves finding  $\mathbf{a}$  minimizing  $\chi^2$ . An NLLSQ problem is therefore an optimization problem whose objective function is  $\chi^2(\mathbf{a})$ .

The Rastrigin function is frequently used for performance testing of optimization methods. Figure 14 shows its 3D surface and contour plots. As can be seen, the function has a global minimum at  $(0, 0)$  and numerous local minima. When handling such a function, an optimization method itself is not guaranteed to converge to the global minimum and often gets "lost" if started far from the solution. Fortunately, setting the guessed values close to the solution greatly improves the convergence. In this paper, such guessed values are obtained through Monte Carlo experiments consisting of the following steps:

1. Estimate the domains of  $a_j$ 's.
2. Create a lot of different combinations of  $a_j$ 's over these domains.
3. Compute the values of  $\chi^2$  for these combinations.
4. Find as many neighborhoods of local minima as possible.



(a) 3D surface.



(b) Contour.

**Figure 14. Rastrigin function.**

The global minimum can be found first by carrying out an optimization procedure at each of these neighborhoods and then by identifying the local minimum yielding the smallest  $\chi^2$ .

Optimization methods can be classified into (1) those only requiring evaluations of the objective functions (e.g., Powell’s method) and (2) those also requiring evaluations of the derivatives of the objective functions (e.g., Newton’s method). In this paper, Powell’s method is chosen due to the following reasons:

- Newton’s method often fails to converge if an  $a_j$  is an exponent.
- In trial and error, it is difficult to compute the derivatives of  $\chi^2$  through FE analysis.
- Given good initial guesses, Powell’s method produces good convergence and high efficiency.

Powell’s method involves successively minimizing the objective function along  $M$  mutually non-interfering directions (see Figure 15 for the case of  $M = 2$ ). These directions are defined so that Powell’s method converges quadratically (see Ref. [22] for more details). The procedure is repeated until the objective function effectively stops decreasing, or mathematically speaking, until

$$|\chi_k^2 - \chi_{k-1}^2| < \varepsilon_1 \quad \text{or} \quad \left| \frac{\chi_k^2 - \chi_{k-1}^2}{\chi_{k-1}^2} \right| < \varepsilon_2, \quad (192)$$

where  $\chi_k^2$  and  $\chi_{k-1}^2$  are the values of  $\chi^2$  in the current and the previous iteration, respectively, and  $\varepsilon_1$  and  $\varepsilon_2$  are two prescribed tolerances.

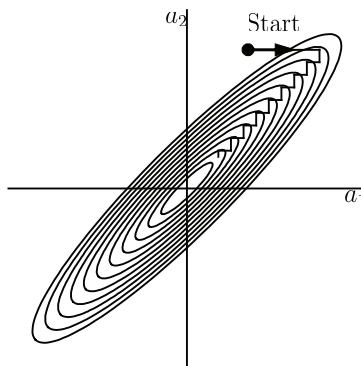


Figure 15. Successive minimizations in a long, narrow “valley” (adapted from Ref. [22]).

## References

- <sup>1</sup>Nguyen, V. D., Lani, F., Pardoën, T., Morelle, X. P., and Noels, L., “A large strain hyperelastic viscoelastic-viscoplastic-damage constitutive model based on a multi-mechanism non-local damage continuum for amorphous glassy polymers,” *International Journal of Solids and Structures*, Vol. 96, 2016, pp. 192–216.
- <sup>2</sup>Gudimetla, M. R. and Doghri, I., “A finite strain thermodynamically-based constitutive framework coupling viscoelasticity and viscoplasticity with application to glassy polymers,” *International Journal of Plasticity*, Vol. 98, 2017, pp. 197–216.
- <sup>3</sup>Krairi, A., Doghri, I., Schalnaf, J., Robert, G., and Van Paepegem, W., “Thermo-mechanical coupling of a viscoelastic-viscoplastic model for thermoplastic polymers: thermodynamical derivation and experimental assessment,” *International Journal of Plasticity*, Vol. 115, 2019, pp. 154–177.
- <sup>4</sup>Miled, B., Doghri, I., and Delannay, L., “Coupled viscoelastic–viscoplastic modeling of homogeneous and isotropic polymers: Numerical algorithm and analytical solutions,” *Computer Methods in Applied Mechanics and Engineering*, Vol. 200, No. 47–48, 2011, pp. 3381–3394.
- <sup>5</sup>Simo, J. C., “Algorithms for static and dynamic multiplicative plasticity that preserve the classical return mapping schemes of the infinitesimal theory,” *Computer Methods in Applied Mechanics and Engineering*, Vol. 99, No. 1, 1992, pp. 61–112.
- <sup>6</sup>Berdichevsky, L. V., *Variational principles of continuum mechanics: II. Applications*, Springer, New York, 2009.
- <sup>7</sup>Yu, W. and Tang, T., “Variational asymptotic method for unit cell homogenization of periodically heterogeneous materials,” *International Journal of Solids and Structures*, Vol. 44, No. 11–12, 2007, pp. 3738–3755.
- <sup>8</sup>Yu, W., “A unified theory for constitutive modeling of composites,” *Journal of Mechanics of Materials and Structures*, Vol. 11, No. 4, 2016, pp. 379–411.
- <sup>9</sup>Zhang, L. and Yu, W., “A micromechanics approach to homogenizing elasto-viscoplastic heterogeneous materials,” *International Journal of Solids and Structures*, Vol. 51, No. 23, 2014, pp. 3878–3888.

- <sup>10</sup>Zhang, L. and Yu, W., “Variational asymptotic homogenization of elastoplastic composites,” *Composite Structures*, Vol. 133, 2015, pp. 947–958.
- <sup>11</sup>Zhang, L., Sertse, H. M., and Yu, W., “Variational asymptotic homogenization of finitely deformed heterogeneous elastomers,” *Composite Structures*, Vol. 216, 2019, pp. 379–391.
- <sup>12</sup>Besson, J., Cailletaud, G., Chaboche, J.-L., and Forest, S., *Non-linear mechanics of materials*, Vol. 167 of *Solid Mechanics and Its Applications*, Springer, New York, 2009.
- <sup>13</sup>Perzyna, P., “Fundamental problems in viscoplasticity,” *Advances in Applied Mechanics*, Vol. 9, Academic Press, 1966, pp. 243–377.
- <sup>14</sup>Holzappel, G. A., *Nonlinear solid mechanics: a continuum approach for engineering*, John Wiley & Sons Ltd., Chichester, 2000.
- <sup>15</sup>Washizu, K., *Variational methods in elasticity and plasticity*, Pergamon press, 1975.
- <sup>16</sup>Rabbat, N., Sangiovanni-Vincentelli, A. L., and Hsieh, H., “A multilevel Newton algorithm with macromodeling and latency for the analysis of large-scale nonlinear circuits in the time domain,” *Circuits and Systems, IEEE Transactions on*, Vol. 26, No. 9, 1979, pp. 733–741.
- <sup>17</sup>Garcia, C. B. and Zangwill, W. I., *Pathways to solutions, fixed points, and equilibria*, Prentice-Hall, Englewood Cliffs, NJ, 1981.
- <sup>18</sup>Zhang, C. and Moore, I. D., “Nonlinear mechanical response of high density polyethylene. Part I: Experimental investigation and model evaluation,” *Polymer Engineering & Science*, Vol. 37, No. 2, 1997, pp. 404–413.
- <sup>19</sup>Holzappel, G. A., “On large strain viscoelasticity: continuum formulation and finite element applications to elastomeric structures,” *International Journal for Numerical Methods in Engineering*, Vol. 39, No. 22, 1996, pp. 3903–3926.
- <sup>20</sup>Voce, E., “A practical strain-hardening function,” *Metallurgia*, Vol. 51, No. 307, 1955, pp. 219–226.
- <sup>21</sup>Simo, J. C. and Taylor, R. L., “Quasi-incompressible finite elasticity in principal stretches. Continuum basis and numerical algorithms,” *Computer Methods in Applied Mechanics and Engineering*, Vol. 85, No. 3, 1991, pp. 273–310.
- <sup>22</sup>Press, W. H., Flannery, B. P., Teukolsky, S. A., and Vetterling, W. T., *Numerical recipes in C: the art of scientific computing*, Cambridge University Press, 1992.